ASCOT/EAGLE Internal Note
MUON-NO-006
1 July 1992

SIMULATION OF MUONS FROM HADRON DECAYS AND HADRON PUNCHTHROUGH FOR ASCOT MUON SYSTEM

A. Cheplakov, A. Kriushin, V. Kukhtin, R. St.Denis

Abstract

The Note[1)] describes current status and the problems in simulation of a hadron decays and hadron punchthrough contribution to the rates of muons which have to be registered by muon chamber system in ASCOT. A brief review of different parameterizations is presented. First results on punchthrough have been compared with existing experimental data. Contribution of hadron decays has been checked using an extrapolation of collider data for minimum bias events.

1 Introduction

A significant contribution to background hits in the ASCOT muon system comes from pion and kaon decays before the calorimeter, decay muons from hadrons in the showers and hadron leakage from the calorimeter system. The first source we refer to as "hadron decays" and the latter two as "hadron punchthrough". To describe all the sources correctly one needs not only detailed GEANT simulation but also a test of the results. This is obtained using published experimental data and their parameterizations.

1) Very early version of the Note was distributed at ASCOT Meeting on 27 April 1992 as "ASCOT NOTE No.9".

The goals of studying hadron punchthrough are a determination of its contribution to muon trigger rates and of occupancies in the ASCOT muon chambers arising from jet events. We have written simple FORTRAN code which allows one to calculate muon chamber occupancies from the above mentioned sources and which can be easy implemented in a fast Monte-Carlo Generator of ISAJET or PYTHIA types.

2 Parameterization of punchthrough probability

A. Bodek [1] was the first to publish a summary of experimental data on hadron punchthrough in different absorbers (calorimeters). Later, K. Lang [2] proposed some formulae for parameterization of muon background in dense calorimeter. A paper by D. Green and D. Hedin [3] devoted to muon rates at the SSC maintains also a simple parameterization of muon spectra in the punchthrough tail as well as a hadron punchthrough probability. F. Lacava [4] compiled published data and presented a parameterization of this probability in terms of the two components (hadronic and muonic). At the LHC Workshop in Aachen in a number of reports punchthrough in hadronic showers was discussed. A detailed Monte-Carlo simulation (for CMS detector) including the punchthrough reduction at the trigger level was presented by H. Fesefeldt [5]. Lastly, there are experimental results on the leakage of hadron showers produced in a lead/scintillating-fiber calorimeter (LAA project) [6].

The most important parameters for punchthrough parameterization are the total thickness of material with an effective absorption length λ_{eff} (which is inversely proportional to the average absorber density) in front of a detection plane and momentum of an incoming to absorber hadron.

The charged hadrons (π/K) decaying in flight generate muons which carry a large

fraction of the parent hadron energy and show a flat momentum distribution in the muon system. The overwhelming majority of incoming hadrons produce showers. Decays of hadrons within the shower produce "soft" muons. In the sample of all particles coming out from the absorber, hadrons from the shower dominate at high initial hadron momenta and small depth of absorber, whereas muons from decays within the shower contribute mainly at low hadron momenta.

F. Lacava [4] proposed the formulae which describe a total punchthrough probability in iron as the function of a hadron momentum $p(GeV/c)$ and an absorber thickness depth $x(cm)$ as:

$$P(p,x) = P_h(p, x/\lambda_{att}) + \chi(\lambda_{eff}) \cdot P_\mu(p, R(x)) - P_{h\mu}, \qquad (1)$$

where $P_h = A(p) \cdot exp(-x/\lambda_{att}(p))$, $[\lambda_{att}(p) = 1/b(p)]$ is the contribution of the hadronic component to the probability; $P_\mu(p, R(x))$ and $\chi(\lambda_{eff})$ follow the parameterization of Lang [2] for muonic component but also includes a factor for extrapolation to any λ_{eff}. Here $R(GeV)$ characterizes the range of the muon from the beginning of the detector, and the functions $A(p)$ and $b(p)$ [4] represent an approximation to the known experimental data. For $P_{h\mu}$ (the probability to have punchthrough muon or hadron) F. Lacava used the following empirical approximation :

$$P_{h\mu} = P_h \cdot \chi(\lambda_{eff}) \cdot P_\mu/(P_h + P_\mu).$$

The P_h parameterization is correct for the probability values ≤ 0.50, and P_μ was obtained for $40 \leq E_h \leq 400GeV$ but can be extended with some uncertainty to lower hadron energies.

Another approximation for hadron punchthrough probability was given by D. Green

[3]. In this case a fit to WA1 data was performed using the following formulae:

$$P(p,x) \approx exp[-(x-x')/\lambda_0],$$

$$x' = 1.53 \cdot p(GeV)^{0.33} \cdot \lambda_{eff}, \tag{2}$$

$$\lambda_0 = 0.89 \cdot p(GeV)^{0.165} \cdot \lambda_{eff},$$

where the punchthrough probability equals to one for depth less than x'.

The level of agreement between the two parameterizations and published experimental data can be seen in Fig. 1. The data were obtained from the E744 experiment [7] for different incident hadron momenta and various absorber thicknesses. One can see from Fig. 1 that the former parameterization (Eq. 1) is more preferable than the latter (Eq. 2) and reproduces experimental data on the dependence of punchthrough probability on the thickness of absorber quite satisfactorily for $p_h \geq 25GeV/c$. The $15GeV$ data are fit best by Green for low absorption thickness ($x \leq 250cm$) but are described better by Lacava above this thickness. The Lacava approach is distinguished by calculation of muonic component which causes a second slope in the probability dependence on initial hadron momenta.

3 Showers Produced by Single Pion in the ASCOT Calorimeter at $\eta = 0$.

We have generated showers from π^+'s using the GEANT(SLUG) Monte-Carlo to simulate a parallel plate LAr calorimeter. Simulation of various energy pions was done for a fixed calorimeter thickness representing that at $\eta = 0$ using the geometry described in the ASCOT Expression of Interest [8]. For the generation with GEANT we have used the version of calorimeter configurations with electromagnetic calorimeter having total

absorption thickness in barrel region of $1.13\lambda_{abs}(\lambda_{abs} = 31cm)$ and hadron calorimeter of $7.7\lambda(\lambda = 18.2cm)$. The electromagnetic calorimeter was composed of 81 layers, each of $0.4cm$ ($0.113cm$ of LAr + $0.140cm$ of copper-cladded G10 + $0.170cm$ of Lead), and hadron calorimeter consisted of 45 $3cm$ - layers ($0.113cm$ of LAr + $0.140cm$ of G10 + $2.8cm$ of Iron). Together with inner/outer cryostats, tail catcher and gaps between the parts of absorber it had a thickness of $318cm$ ($13.5\lambda, \lambda = 23.56cm$).

The results of data processing are summarized in Table 1. Fig. 2 shows the values of the punchthrough probability in ASCOT derived in this simulation. The values were calculated as the ratio of the number of events where at least one hit was observed in the first muon plane to the total number of generated pions. The probabilities obtained (closed circles) are compared with the Lacava and Green parameterizations, and a satisfactory agreement is seen for pions with $p \geq 40GeV/c$ (see Table 1 for detailed comparison with Lacava parameterization). Open circles in Fig. 2 reproduce the result of probability calculation when we have corrected the number of the "punchthrough events" by subtracting the estimated number of initial pion decays before the inner surface of barrel calorimeter ($L_{decay} = 160cm$). Thus, the probability values were visibly decreased for low hadron momenta. The corrected number of events also are presented in the Table 1.

Table 1: Results of ASCOT/GEANT simulation on punchthrough probability for different single pion momenta.

$p_{\pi+}$ $(GeV/c$	N_{tot}^{event}	N_{punch}^{event}	N_{corr}^{event}	$Prob_{punch}$	F.Lacava parameterization
10	20K	142	85	$(4.3 \pm 0.1) \cdot 10^{-3}$	$0.4 \cdot 10{-}3$
20	10K	90	76	$(7.6 \pm 0.1) \cdot 10^{-3}$	$2.7 \cdot 10{-}3$
40	10K	169	162	$(1.6 \pm 0.1) \cdot 10^{-2}$	$1.2 \cdot 10{-}2$
60	10K	210	205	$(2.1 \pm 0.1) \cdot 10^{-2}$	$2.3 \cdot 10{-}2$
100	15K	611	607	$(4.0 \pm 0.2) \cdot 10^{-2}$	$4.9 \cdot 10{-}2$
200	3K	256	256	$(8.5 \pm 0.5) \cdot 10^{-2}$	$10.8 \cdot 10{-}2$
300	3K	359	359	$(12.0 \pm 0.6) \cdot 10^{-2}$	$15.8 \cdot 10{-}2$
500	1K	212	212	$(21.2 \pm 1.5) \cdot 10^{-2}$	$23.8 \cdot 10{-}2$

3.1 Punchthrough probabilities at low hadron momenta

Fig. 2 also shows a disagreement of the obtained probabilities with the parameterizations for incident pion momenta below $30 GeV/c$. We have to note that for low hadron momenta the parameterization does not give a valid prediction because of the lack of experimental data. Conceivable reasons for the mentioned discrepancy have to be investigated since the data of E744 experiment [7] (open square) confirm the Lacava parameterization.

An obvious calorimeter feature which may cause the increased punchthrough contribution to the muon chamber occupancy is the presence of a significant volume free of dense material. We have studied this problem by generating showers induced by single π^+-mesons of 10 GeV/c and 20 GeV/c momenta traversing electromagnetic (ECAL) and hadron (HCAL) calorimeters. For this purpose we used the latest version of ASCOT calorimeters with total thickness (including tail catcher) of $245cm$ ($12.5\lambda_{eff}$). Two configurations were treated : one without a gap between the electromagnetic and hadron compartments and another one with a $10cm$ gap between the calorimeters. Results of our analysis are presented in Table 2.

For every case 70.000 showers were generated. In Table 2 N_{punch}^{event} indicates the number of events with at least one hit observed in the first muon chamber. The number of events $N_{corr.}^{event}$ were obtained correcting data to account for primary pion decays; the corresponding punchthrough probabilities also are presented. To subtract events including a muon from incident pion decay we used the calorimeter responce. We eliminated events from the analysis if they showed minimum ionizing loss inside both the electromagnetic and hadron calorimeters ($\Delta E_{ECAL}, \Delta E_{HCAL} < 35$ MeV)[2], and had a muon with a mo-

2) Energy losses of decay muons were observed to peak at the value about 20 MeV.

mentum consistent with decay kinematics (with respect to muon energy losses in the absorber we used cut for $p_\mu > 2.5$ GeV/c for pions of 10 GeV/c and $p_\mu > 8.5$ GeV/c for 20 GeV/c pions).

Table 2: Summary results on punchthough probability calculation for low momenta hadrons.

p_{π^+} (GeV/c)	Configu-ration	N^{event}_{punch}	N^{event}_{corr}	$Prob_{punch}$ $\times 10^{-3}$	Paramete-rization	CUT1 $(15MeV)$	CUT2 $(25MeV)$	CUT3 $(40MeV)$
10	no gap	340	114	(1.6 ± 0.2)	$0.5 \cdot 10^{-3}$	$2.7 \cdot 10^{-3}$	$2.1 \cdot 10^{-4}$	$0.7 \cdot 10^{-4}$
10	$10cm$	333	140	(2.0 ± 0.2)	$0.7 \cdot 10^{-3}$	$2.7 \cdot 10^{-3}$	$2.3 \cdot 10^{-4}$	$0.7 \cdot 10^{-4}$
20	no gap	448	348	(5.0 ± 0.3)	$5.5 \cdot 10^{-3}$	$5.0 \cdot 10^{-3}$	$2.0 \cdot 10^{-3}$	$1.1 \cdot 10^{-3}$
20	$10cm$	449	363	(5.2 ± 0.3)	$7.5 \cdot 10^{-3}$	$5.2 \cdot 10^{-3}$	$2.0 \cdot 10^{-3}$	$1.2 \cdot 10^{-4}$

In the frame of statistical uncertainties for $10cm$ gap we have observed no significant increasing of punchthrough probabilities for 10 GeV/c and 20 GeV/c incident pions.

The inhomogeneity of our absorber may also cause disagreement of obtained probability values with the Lacava parameterization. The interaction length value for electromagnetic calorimeter placed in front of absorber is about 1.7 times greater than that of the hadron calorimeter. It may result in increase of the decay muon contribution in comparison with standard homogeneous absorbers used in fixed - target experiments from which data were taken by F.Lacava to obtain the punchthrough probability parameterization (for 10 GeV/c pions without the gap we observed 25% excess over estimated number of decay muons).

Data presented in Table 2 elicidate another possibility that explains the discreapancy at low hadron momenta. In our calculation with GEANT we used for simplicity a thick ($2mm$) scintillator layer instead of a complex description of muon chambers. Every charged particle leaving the scintillator was recorded as individual hit. Experimentally, to register a shower in the calorimeter as well as to eliminate the muon mixture in the hadron beam, one usually sets some threshold on the calorimeter signal. Three last columns of

Table 2 illustrate the influence of different cuts for calorimeter responce (both ECAL and HCAL) on the punchthrough probability values. We subtracted from the N_{punch}^{event} those events having a low ionization inside the calorimeters. It is seen that the signal threshold influence is much more significant for lower hadron momenta.

Thus, the discrepancy in the obtained and estimated punchthrough probability values can be explained by specific features of the calorimeter configuration as well as the hit determination used in the experiment. By the way, in the case of significant disagreement with known parameterization and/or experimental data one should modify the parameterization taking into account the experiment features or estimate the uncertainty level due to the lack of valid information.

Better agreement of the Lacava parameterization with GEANT results at high pion momenta, where decay contribution became negligible, allows us to use parameterization (Eq. 1) for hadron punchthrough probability calculations.

3.2 Some features of hadron leakage

The charged particle flow into the ASCOT muon system consists of low energy electrons (positrons), as well as muons and hadrons. Neutrons escaping the absorber may also cause hits due to secondary (mainly elastic) interactions. Table 3 shows muon and hadron production probabilities as well as their average multiplicities and momenta in the punchthrough events (after subtracting decay muon contributions).

Fig. 3 shows the contribution of the different charged secondaries and corresponding momentum spectra for initial pions with $p_{\pi^+} = 20 GeV/c$ (70K generated events) and Fig. 4 for $100 GeV/c$ (15K events) at $\eta = 0$. Both bremsstrahlung and π^0-decays contribute to the momentum spectrum of electrons and positrons. Some attention should also be paid

Table 3: Some average characteristics of hadron leakage for different single pion momenta (ASCOT/GEANT simulation). Statistics is the same as presented in Table 1.

$p_{\pi+}(GeV/c)$	N^{event}_{punch}	$Prob_\mu(\%)$	$Prob_h(\%)$	$< n_\mu >$	$< p_\mu >$	$< n_h >$	$< p_h >$
10	85	$.13 \pm .03$	$.01 \pm .01$	$.29 \pm .07$	3.6 ± 0.2	$.02 \pm .02$	$.02 \pm .02$
20	76	$.14 \pm .04$	$.22 \pm .05$	$.18 \pm .06$	7.1 ± 1.1	$.29 \pm .07$	2.8 ± 0.8
40	162	$.32 \pm .06$	$.75 \pm .09$	$.20 \pm .04$	8.9 ± 2.0	$.46 \pm .06$	1.9 ± 0.5
60	205	$.34 \pm .06$	1.7 ± 0.1	$.17 \pm .03$	8.1 ± 2.1	$.85 \pm .09$	1.6 ± 0.2
100	607	$.79 \pm .07$	3.1 ± 0.1	$.20 \pm .02$	6.4 ± 2.5	$.75 \pm .05$	1.5 ± 0.6
200	256	1.4 ± 0.2	9.7 ± 0.6	$.16 \pm .03$	6.8 ± 4.5	$1.14 \pm .10$	2.3 ± 0.4
300	359	1.6 ± 0.2	16.0 ± 0.7	$.13 \pm .02$	3.4 ± 1.0	$1.34 \pm .09$	2.9 ± 0.4
500	212	3.6 ± 0.6	29.1 ± 1.7	$.17 \pm .03$	1.6 ± 0.2	$1.37 \pm .12$	3.3 ± 0.7

to the effect of particle circulation in the magnetic field after the particle exits the end of the calorimeter. It is significant for low momenta electrons and positrons. The muon momentum spectrum for $20GeV/c$ pions at high values of p_μ reveals a plateau which indicates a visible contribution of pion decays at low π^+ momenta. At $p_{\pi+} = 100GeV/c$ the contribution of the shower particle decays to the muon spectrum dominates. The multiplicity of secondary particles grows with initial hadron energy. The dependence of the probability to create an escaping muon (corrected for initial pion decays) on the parent pion momentum is shown in Fig. 5 a. The linear behaviour (we have obtained the slope value $6.2 \cdot 10^{-5}$ $\%/GeV/c$ with χ^2/d.f. $= 1.5/6$) agrees with the experimental data [6] on shower leakage in the calorimeter with a thickness of 9.6 nuclear interaction lengths (the slope of the curve that they presented was $1.3 \cdot 10^{-4}$ $\%/GeV/c$). We also agree with the data [6] on the relative yield of hadrons (Fig. 5 b) which is about ten times greater that that of muons.

For the sample of events having at least one hit in the ASCOT muon system, the dependences of the average muon and average hadron multiplicities on the initial hadron momenta were obtained and are shown in Fig. 5 c and d. The solid lines represent fits to the data. The muons have a constant multiplicity whereas the hadrons have a logarithmic dependence on initial hadron momentum approximated by constant value for muons and

by a smoothing curve for hadrons (Fig. 5 c and d).

The momentum spectrum of escaping muons has been measured relatively poorly. A parameterization of data from two experiments (Lab E neutrino experiment (unpublished) and E-379 Fermilab experiment [2]) is presented in paper [3]. The data were obtained in an interval of incident hadron energies from 40 to 225 GeV. The probability to find muon at a momentum fraction z of the hadron is given as sum of two exponentials:

$$D_\mu(z) \approx a_1 e^{-b_1 z} + a_2 e^{-b_2 z} \tag{3}$$

The authors demonstrated in the paper (see Fig. 6) that two data sets for various types of hadrons together with the hadron energies agreed. Small statistics does not allow us to fit the muon momentum spectra separately for different $p_{\pi+}$. So, Fig. 7 shows a two - exponential fit of the hadron "fragmentation function" for the sum over all muon spectra. To avoid significant contribution from decaying pions we used data only for $p_{\pi+} \geq 60$ GeV/c and rejected muons with the hadron momentum fraction $z \geq 0.2$. The obtained function has been compared with data mentioned in Fig. 6, and qualitative agreement with the data is observed.

We therefore have the tools necessary to calculate cross sections for secondary particles due to punchthrough. There are two strategies available. In the first ("STRATEGY 1") we use the muon/hadron production probability (Fig. 5 a and b) (which incorporates punchthrough probability with multiplicity) together with the fit of the hadron fragmentation function. In second ("STRATEGY 2") we use the parameterization for initial hadron punchthrough probability together with the average muon/hadron multiplicities (Fig. 5 c and d) and the fit of the hadron fragmentation function ("FRAGM1"). All the parame-

ters were obtained at $\eta = 0$, which corresponds to the minimal total absorption length. So, application of these values at other η's should not underestimate the muon rates. Because of the lack of statistics we have not investigated dependence of the shape of the fragmentation functions on multiplicity of secondaries.

4 ISAJET plus hadron punchthrough probabilities

To deal with minimum bias events we have generated using ISAJET a sample of TWOJET events with the lower limit on p_T^{JET} chosen to give a cross section equal to the minimum bias inelastic cross section (see ISAJET 6.34 Manual). As far as expectation for the LHC is $\sigma_{tot} = (110 \pm 20)mb$ and $\sigma_{el}/\sigma_{tot} \approx 0.26$ (see ref. [9], [10]) we estimate $\sigma_{inel} = (70 \div 100)mb$ and used two values for the lower limit of p_T^{JET} : 3.3 and 4.0 GeV/c. Using ISAJET we generated two - jet events with option "ALL". For each of 22 intervals for the jet transverse momentum $(3.3(4.0) \div 5, 5 \div 10, 10 \div 15, \ldots 30 \div 40, 40 \div 50, 50 \div 75, \ldots 200 \div 250, \ldots 550 \div 600$ GeV/c) 2000 events were generated. This generation resulted in total Monte-Carlo cross section of 102 (70) mb, with 59 (27) mb coming from the $3.3(4.0) \div 5 GeV/c$ generation. Thus, we can analyse the effect of cross section uncertainty. In addition, we also used 3.8 GeV/c - cut for p_T^{JET} which resulted in $\sigma = 79mb$ closed to the prediction of PYTHIA for minimum bias event cross section ($80mb$).

Then we have used a simple simulation to consider muon production from the following "stable" (ISAJET terminology) hadrons:

$$\pi^{\pm},\ \pi^0,\ K^{\pm},\ K^0_{S,L},\ p,\ \overline{p},\ n,\ \overline{n},\ \Lambda^0,\ \overline{\Lambda^0}.$$

The simulation has the following features (see Fig.8 for geometrical details) :

1. The original particles are tracked in a central cavity having a $1.5T$ magnetic field

and dimensions $R_{in} = 1.4m, Z_{in} = 2.55m$. The particles with low transverse momentum $p_T \leq 60 MeV/c$ which corresponds to one half of the forward hole radius were not considered.

2. Hadron decays were generated assuming two - particle mode with corresponding branching ratios and the lifetimes of the mesons. Only hadrons with direct branching to muons were decayed.

3. The momenta of muons produced in the decays were decreased in accordance with specific minimum ionizing energy losses, (195 MeV/λ). Therefore $p_{min} = 2.6\ GeV/c$ at $\eta = 0$ and low momenta muons were "absorbed". The muons from the hadron decays were stored in the histogram with weights which were equal to the calculated probability of the hadron decay, P_{decay}.

4. For the hadrons striking the calorimeter we have calculated the punchthrough probability, P_{punch}, using F.Lacava parameterization and a tube shaped calorimeter encompassing the inner cavity and having dimensions:

$$R_{in} = 1.4m, \quad Z_{in} = 2.55m, \quad R_{out} = 4.66m, \quad Z_{out} = 6.35m.$$

We assumed zero value of magnetic field inside homogeneous calorimeter with averaged absorption length 27.16 cm. The input parameters for punchthrough calculation were momenta of the particles and their potential range inside the material of the calorimeter. To obtain the muon/hadron momentum spectra we have used the strategies mentioned above and stored the momentum of the muon/hadron in histogram with weight $w = P_{prod} \cdot (1 - P_{decay})$ for "STRATEGY 1" and $w = P_{punch} \cdot (1 - P_{decay}) \cdot N$ for "STRATEGY 2", where N is the muon/hadron multiplicity generated with Poisson statistics having

mean value given by the parameterization of Fig. 5 (c and d).

We have to note that there are a few methods to generate a sample of minimum bias events. So, in paper [11] a good agreement with experimental data was shown when 32% of hard scattering events were mixed to ISAJET MINBIAS generation.

5 Analysis of the momentum spectra of generated muons

The results have been presented in a series of pictures: Fig. 11 - Fig. 16, obtained for minimal $p_T^{JET} = 3.8\ GeV/c$ $(\sigma = 79mb)$.

The effect of different "cut-off" criteria is shown for rapidity spectrum of secondary hadrons in Fig. 9 a and b. Solid line in Fig. 9 corresponds to initial spectra, whereas dotted one reproduces spectrum of hadrons striking the calorimeter, i.e. having at the endcaps $(Z = 2.6m)$ the geometrical $\mid \eta \mid \leq 3$. A gap at small η is due to magnetic field influence on low momentum hadrons curling to the holes at endcaps of the calorimeter. Note that contribution of charged pions shown by dashed - dotted line reproduces well known [11] value of about 7 per unit rapidity (Fig. 9 b). Fig. 10 (a and b) demonstrates a weak dependence of hadron transverse momentum spectrum on the "cut-off" criteria.

In Fig. 11 we show the momentum spectrum of the hadrons which were generated using ISAJET in two-jet events and were used for calculation of muon production in hadron punchthrough and through the decays. Fig. 12 illustrates the influence of the calorimeter absorption power on differential muon momentum spectra from hadron decays. The most significant effect is observed for low momentum muons produced in central rapidity region: cross sections decrease by about four orders of magnitude. The resulting integrated spectra of muons and secondary hadrons in different rapidity intervals are shown in Fig. 13. The total muon momentum spectrum is a sum of primary hadron decays

and of hadron punchthrough contribution. In minimum bias events the contribution of muons is greater than that of secondary hadrons by about 2 orders of magnitude.

The comparison of two sources of secondary muons (primary hadron decays and hadronic showers) is presented in Fig. 14. The punchthrough contribution is compatible with that from decays only for very low muon momenta ($0 \div 0.5\ GeV/c$). At $\mid \eta \mid \leq 2$ the contribution from hadron punchthrough to low momenta part of muon spectrum is significantly higher than that from hadron decays.

The muon yields from different sources are compared in Fig. 15 (differential cross section) and Fig. 16 (integrated one) where the contributions to the total muon spectrum are also shown for $b-, c-$ and t- quarks decays. It is seen that at low muon momenta hadron decays as well as the punchthrough effects including the appearance of secondary hadrons of hadron shower tails should be taken into account.

5.1 Uncertainties in the Monte-Carlo calculations

Uncertainties in the calculations are presented in Fig. 17 - Fig. 21 and are estimated as follows.

1) Uncertainties due to knowledge of the fragmentation function. The calculation of punchthrough contribution was performed using hadron fragmentation function shown in Fig. 6, Fig. 7 and marked as "FRAGM1". At the low level of statistics which we have used the result of two-exponential approximation significantly depends on selection of the z-interval value and/or histogram dimensions. We have marked as "FRAGM2" the hadron fragmentation function which was obtained using some different parameters of the histogram than those in Fig. 7. As it is seen in Fig. 17 the uncertainties in the hadron fragmentation function could result in significant under/overestimation of

secondary muon yield at the momenta range over 5 GeV/c. We have used also fragmentation function ("D(z)") obtained fitting upper limit of the existing experimental data presented in Fig. 6 (dashed line). Fig. 18 demonstrates comparison of differential and integrated cross sections obtained with two functions usage : "FRAGM1" and "D(z)". It is seen that the situation is very similar to those presented in Fig. 17 and the main contribution to the cross section coming from the low momentum muons is about 4 order of magnitude. The uncertainty in the integrated cross section is about 25 % which is determined by the uncertainty in muon production probability, and it is greater for higher muon momenta.

2) Uncertainties in production probability. The comparison of two strategies for muon spectra calculation is shown in Fig. 19. The dashed line reproduces the resulting muon spectrum when we have used a Poisson distribution to calculate the number of secondary muons in the events which produce any hit in ASCOT muon system. The muon production probability parameterization (Fig. 5 a) which we have obtained at $\eta = 0$ overestimates muon yield. To estimate the uncertainty level we used the parameters error bars of dependencies presented in Fig. 5 a. For different hadron momenta we had uncertainty in the muon production probability about $(10 \div 20)\%$. Using linear approximation of the known experimental data [6] at 9.6λ of total absorption length we can estimate the uncertainty due to ignoring of λ - dependence at the level of 50 %. Thus, one can get about $1 \div 2$ order of magnitude uncertainty in muon rate from the hadron punchthrough because of the absence of valid information about hadron fragmentation function and the λ-dependence of the relevant parameters.

Fig. 20 illustrates the uncertainty in the calculation of hadronic component of shower leakage. The difference in the yield of secondary hadrons is significantly lower that in the

case of muons.

3) Uncertainty in the value of inelastic cross section. At last, Fig. 21 shows the effect of uncertainty in the expected value of minimum bias cross section (about 20%). The muon momentum spectra are scaled with the value of cross section and it should not amount to visible uncertainties in the muon rates calculation.

6 Rates of muons leaving the calorimeter

The coordinates of outgoing particles were calculated based on the hadron (decay muon) position at inner surface of calorimeter after particle curling in the magnetic field of the inner cavity (in the case of charged particles). We supposed zero magnetic field inside the calorimeter and considered the straightline trajectories of particles.

Fig. 22 and Fig. 23 show different projections of the cross section of charged particles (as of decay muons and of hadrons) on the inner and on the outer surfaces of endcap calorimeter. Whereas Fig. 24 and Fig. 25 reproduce three-dimension plots of coresponding rates. At $\eta = 3$ we obtained rates values about $4MHz/cm^2$ at inner surface and $4KHz/cm^2$ at outer surface.

Fig. 26 shows summary on rates of charged particles at barrel surfaces of calorimeter and Fig. 27 exhibits the rates at the endcaps. Note, that for radial distribution a normalization factor of $(1/2\pi R)$ was taken into account to represent rates in $[1/cm^2]$ units.

Fig. 28 demonstrates the results of the rate calculation at the endcaps if the additional $5m$ of iron would be installed after the calorimeter. In this case for homogeneous absorber we have to use the value of absorption length $\lambda = 20.3cm$. So, total absorption length at the endcaps was about 43λ. One can see in Fig. 29 that additional $5m$ length

iron absorber gives factor $10 \div 20$ for decreasing of muon rate at high rapidity values.

Muons from hadron decays give the overhelming contribution to the occupancy of muon system. W.Blum [12] proposed a straightforward method to calculate rates of decay muons on the endcaps assuming that we can use normalized probability distribution $f(p_T)$ for pions which follows the approximation of CDF experimental data:

$$f(p_T) = C \cdot p_T/(p_T + a)^n. \tag{4}$$

Where $C = a^{n-2} \cdot (n-1) \cdot (n-2)$ and $a = 1.29\ \ GeV/c,\ \ n = 8.8$. Average transverse momentum of charged pions at 16 TeV in ISAJET/TWOJET option with p_T^{JET} - cut of 3.8 GeV/c is equal to 0.48 GeV/c, so we have used in Eq. 4 parameters $a = 1.4, n = 8.8$, and average pion multiplicity about 50 at $\mid \eta \mid \leq 3$ ($< \Delta N_\pi/\Delta\eta > = 8$). Thus, to calculate decay muon rates on the endcaps at the distance Z (along the beam) from the vertex and at the polar angle θ one has to estimate the value of the calorimeter absorption power (P_{cut}) and obtain the reduction factor

$$g = \frac{1}{(1 + P_{cut} \cdot \sin\theta/a)^{n-1}}, \tag{5}$$

and then calculate the number of muons per area ΔF as

$$\frac{\Delta N_\mu}{\Delta F} = \frac{n-2}{a} \cdot \frac{m_\pi L_{decay}}{c\tau} \cdot < \frac{\Delta N_\pi}{\Delta\eta} > \cdot \frac{\cos^2\theta}{2\pi Z^2 \sin\theta} \cdot g. \tag{6}$$

The usage of $p_T^{JET} > 3.8\ \ GeV/c$ for TWOJET option of ISAJET gives $\sigma_{inel} = 79mb$ which results in about 2 events per nanosecond at the luminosity $L = 2 \cdot 10^{34} cm^{-2} s^{-1}$. Thus, after $L_{decay} = 2.55m$ and total absorption length of 14λ we obtained at the endcaps of

calorimeter ($Z = 6.35m$) about $4KHz/cm^2$ at $\eta = 3$. Fig. 30 shows a comparison of the muon rates from pion decays obtained with the fast Monte-Carlo program and using Eq. 6. A satisfactory agreement is observed for any radius value and for both 14λ and 43λ absorber configurations.

7 Conclusions

Thus, we can reproduce the general features of the hadron punchthrough and muon rates in ASCOT muon system. The comparison with the known experimental data qualitatively confirms the validity of our calculations. The calculations can be performed for another absorbers with different configuration, one just has to determine the geometrical dimensions and effective absorption length.

Nevertheless, some questions still require additional investigations and full description of the ASCOT detectors in frame of GEANT :

• checking of results for single hadron with the ASCOT/GEANT responce to jets of 40, 100, 300 and 500 GeV energies.

The particle composition of jets should be also investigated. In paper [2] the muon yields from showers initiated by kaons, protons and neutrons were obtained by correcting the results for pions using the factors 1.8, 0.39 and 0.78, respectively. It comes to 3% decrease in the total muon yield as compared to the case where the contributions from all secondaries are assumed to equal that of pions. We do not use this correction in our analysis.

• increasing of statistics to provide high validity of the hadron fragmentation functions (both: for muons and for hadrons).

The independence of hadron fragmentation function on primary hadron momenta

should be confirmed. In addition, for the hadron component of punchthrough the average multiplicity is greater than one. This implies that there are many cases where multiple hadrons punch through. Correlations in the fragmentation of multiple hadrons are expected to be weak and have not been taken into account. At the same time the dependence of the secondary hadrons contribution on the total absorption length has to be clarified.

• the dependence of obtained parameterizations on total absorption thickness should be studied in detail.

Fig. 31 demonstrates an absorbption power of the ASCOT detector including the barrel and endcap calorimeters and tail catcher versus the rapidity of emitted particles. The total absorption length changes from 12λ till $18\lambda(\lambda = 17.1cm)$ for $\eta = 0$ and $\eta = 1$, correspondingly. At the same time the punchthrough probability for pion of 100 GeV/c total momenta decreases from 0.05 to 0.007.

• contribution of the charged (and neutral) hadron component to the occupancy of the muon system.

To confirm the necessity of the latter point the experimental data presented in paper [6] can be reviewed. The yeilds of hadrons and neutrons from the calorimeter were measured, and neutrons were observed about 10 times as often as muons. Escaping hadrons dominate muons for energy of primary hadrons above 20 GeV.

• the influence of magnetic field and the trigger concept on punchthrough rates.

H. Fesefeldt [5] has shown that in the case of CMS detector, combining the effect of strong magnetic fields with a fast time gate in the trigger, the secondary decay muons and the hadron punchthrough can be reduced by approximately 2 order of magnitude.

The contribution of particle circulation in the magnetic field after they coming from

the calorimeter to the occupancy of the ASCOT muon system should be investigated versus the distance to the first chamber.

References

[1] A. Bodek, "Punchtrough in hadron shower cascades, muon identification, and scaling laws for different absorbers", UR-911, Rochester, New York,1985.

[2] K. Lang, "An Experimental Study of Dimuons Produced in High Energy Neutrino Interactions", Ph.D.Thesis, UR-908, Rochester, New York, 1985; K. Lang et al., "Neutrino Production of Dimuons", Z.Phys.C33 (1987) 483.

[3] D. Green and D. Hedin, "Muon rates at the SSC", FERMILAB-Pub-90/18.

[4] F. Lacava, "Punchthrough in hadronic showers: a parameterization of the total probability", ROM-NI 968, 18 Dicembre 1990.

[5] H. Fesefeldt, "Punch Through Simulations", Proc.LHC Workshop, Aachen,4-9 October 1990, v.III,p.457.

[6] D. Acosta et al., "On muon production and other leakage aspects of pion absorption in a lead/scintillating-fiber calorimeter", NIM, A309 (1991) 143.

[7] F.S. Merrit et al., "Hadron Shower Punchthrough For Incident Hadrons of Momentum 15, 25, 50, 100, 200 and 300 GeV/c", NIM, A245 (1986) 27.

[8] ASCOT Collaboration, Expression of Interest, Proceedings of the General Meeting on LHC Physics and Detectors, p.137, 5-8 March 1992, Evian-les-Bains, France.

[9] D. Denegri, "Standard Model Physics at the LHC (pp collisions)", Proc.LHC Workshop, Aachen,4-9 October 1990, v.I, p.56.

[10] C. Bourrely, J.Soffer, Tai Tsun Wu, "Impact picture predictions for pp and pp elastic scattering at CERN collider, FNAL collider, LHC and SSC", Z.Phys.C37 (1988) 369.

[11] G. Ciapetti and A. Di Ciaccio, "Monte Carlo Simulation of Minimum Bias Events at the LHC Energy", Proc.LHC Workshop, Aachen,4-9 October 1990, v.II, p.155.

[12] W. Blum, Private communication, May 1992.

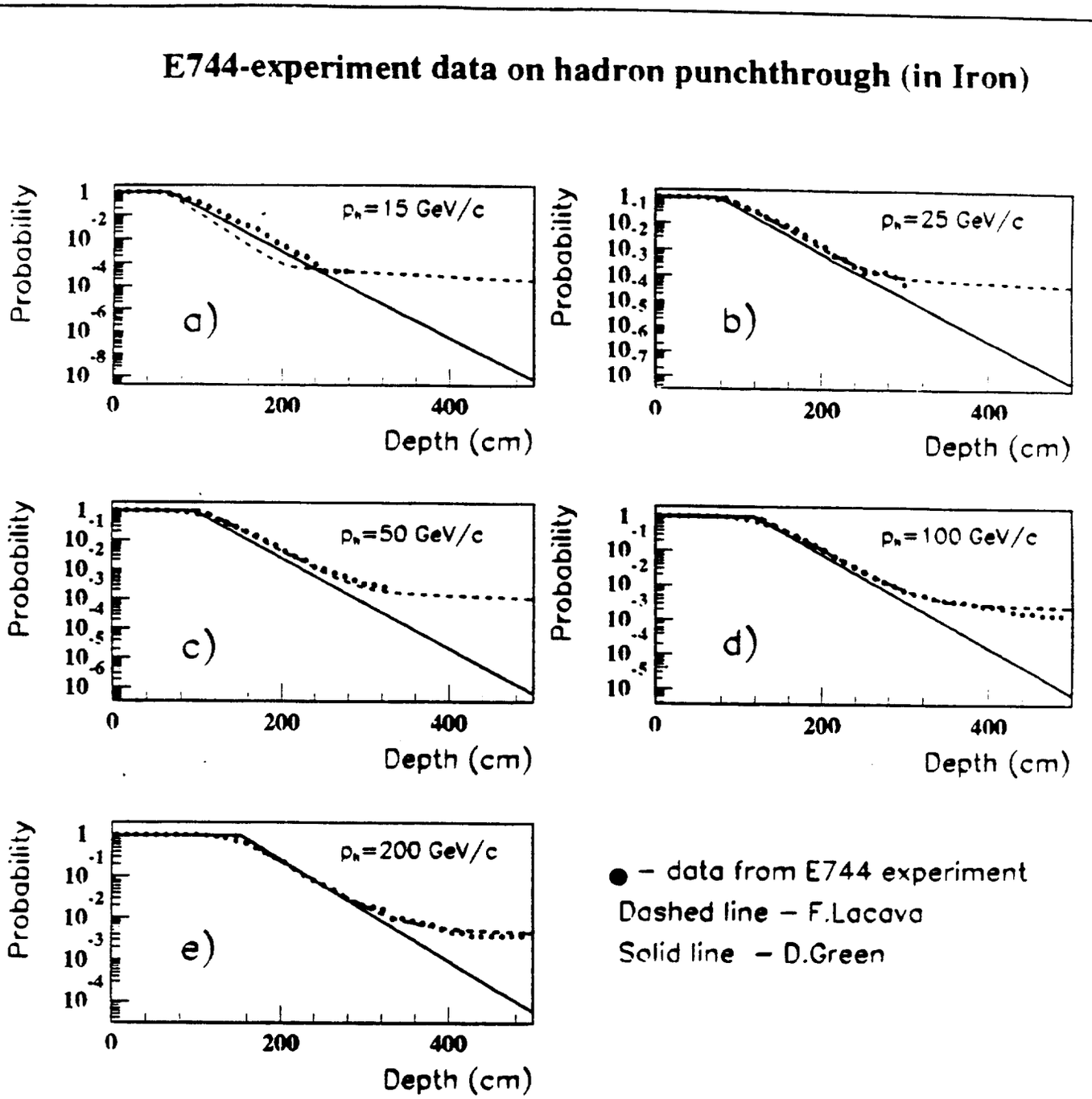

Figure 1: Comparison of both: Lacava (dashed line) and Green (solid line) parameterizations with data of E744 experiment at different hadron momenta ($p_h = 15(a), 25(b), 50(c), 100(d)$ and $200(e) GeV/c$).

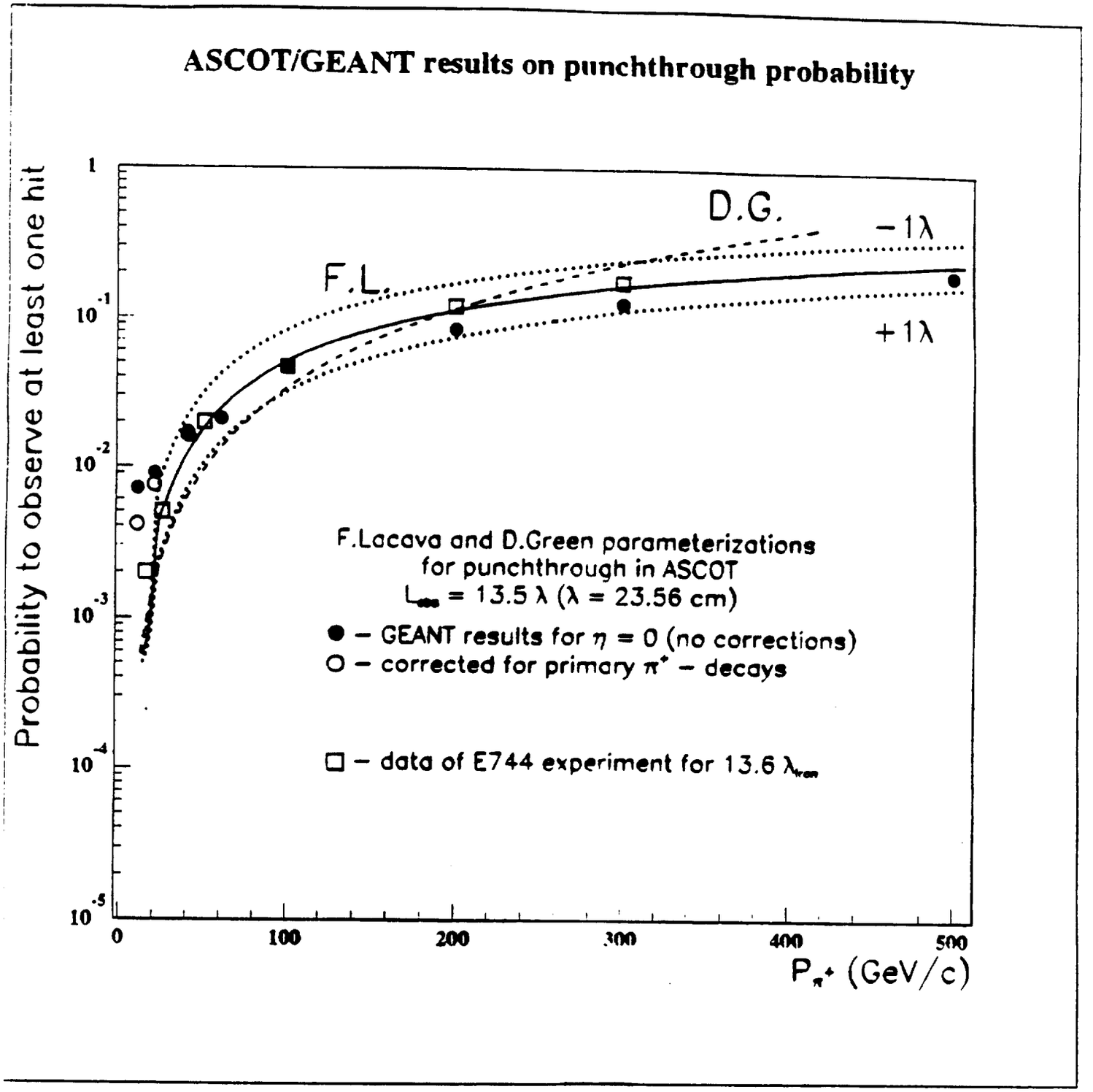

Figure 2: Probability to observe any hit in ASCOT muon system (GEANT calculations) in comparison with Lacava parameterization.

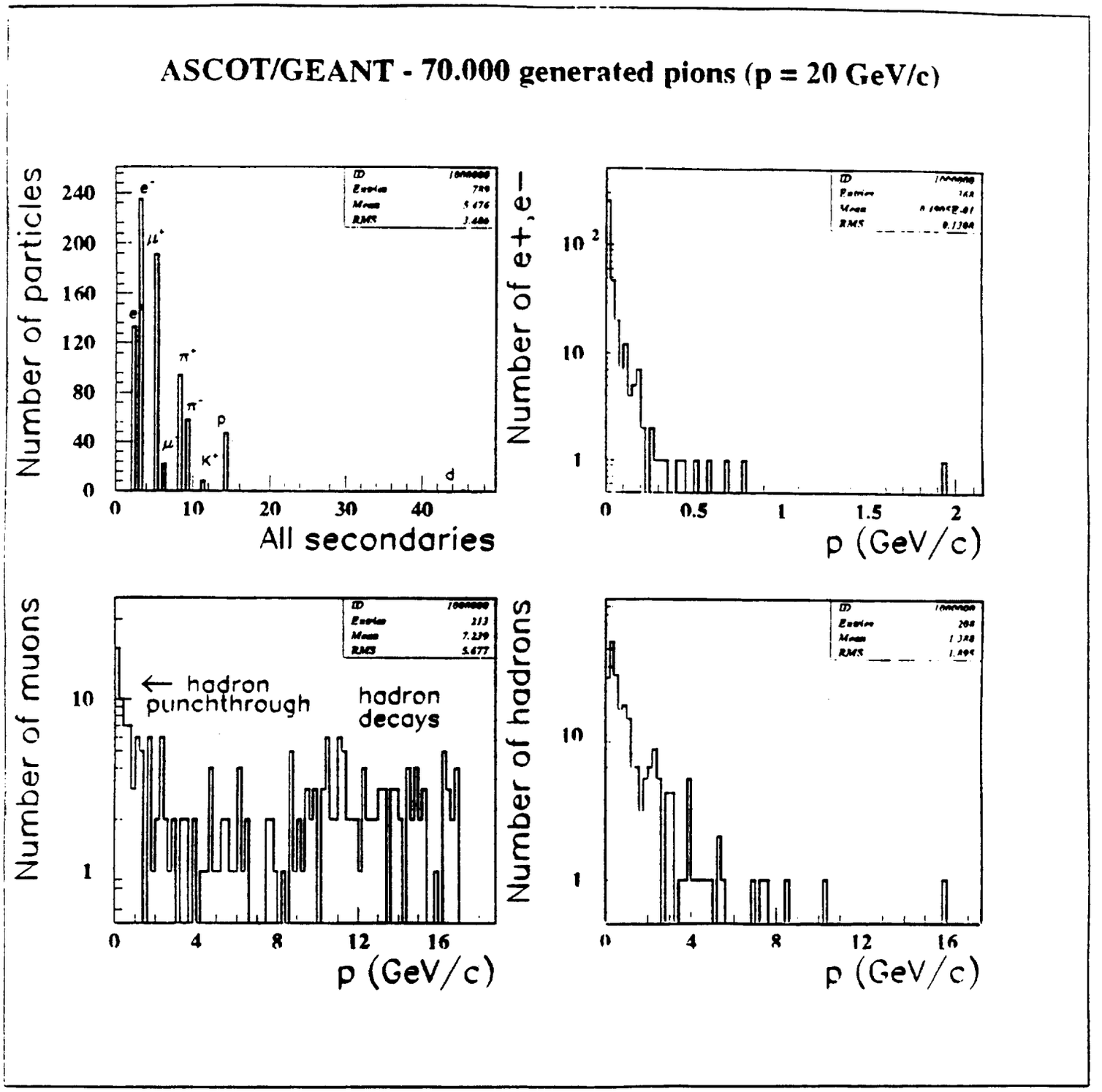

Figure 3: Results of GEANT simulation for secondary particles in first muon chamber. The particles were emitted during the development of the showers caused by single pions with initial momentum 20 *GeV/c*.

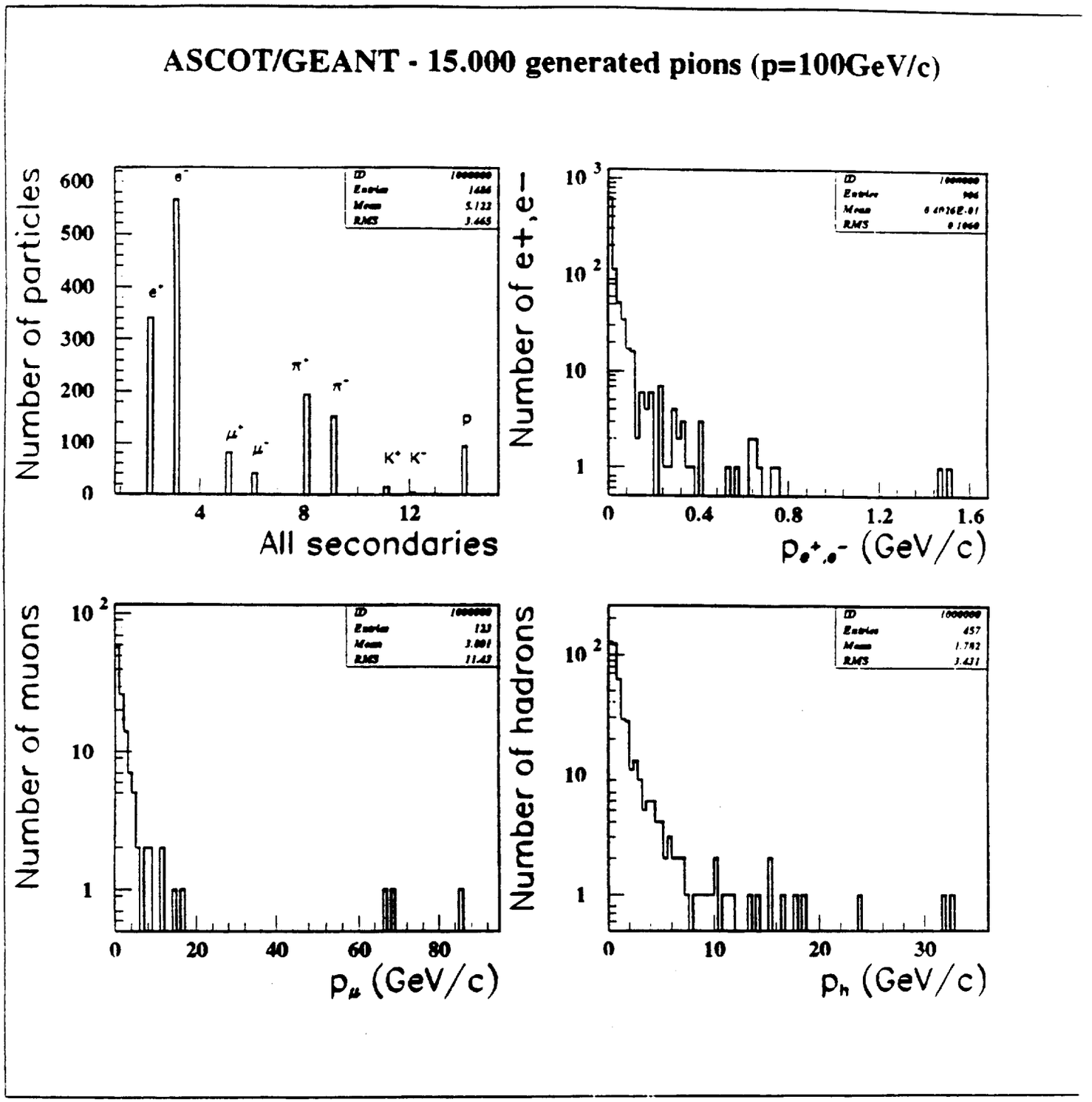

Figure 4: Secondary particles of the hadron showers leakage induced by pions being generated with 100 GeV/c initial momentum.

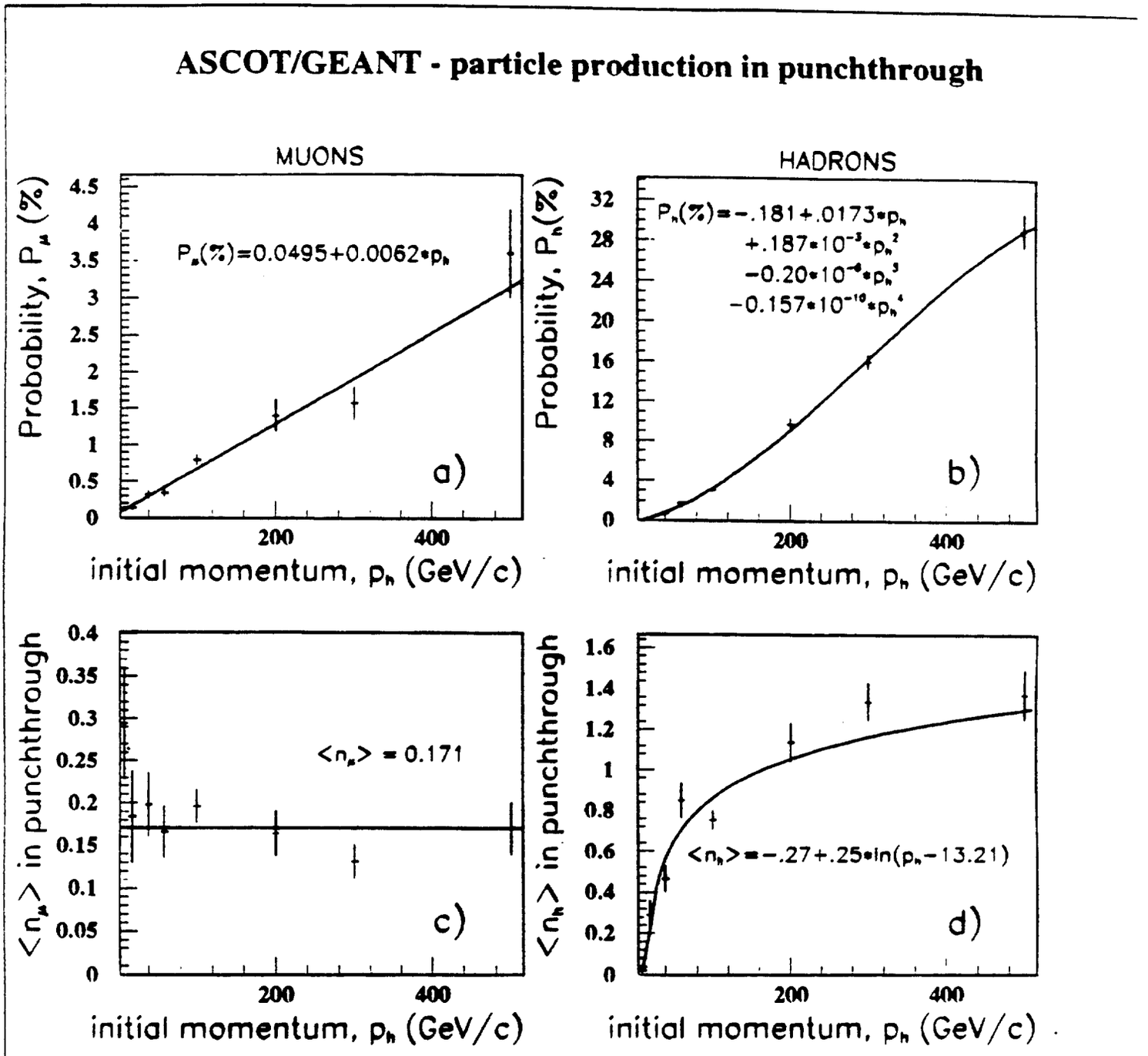

Figure 5: Summary of GEANT results for the probability of muon (a) and hadron (b) production as well as for average particle multiplicities (c and d) versus initial hadron momenta. Parameters of approximations are also presented.

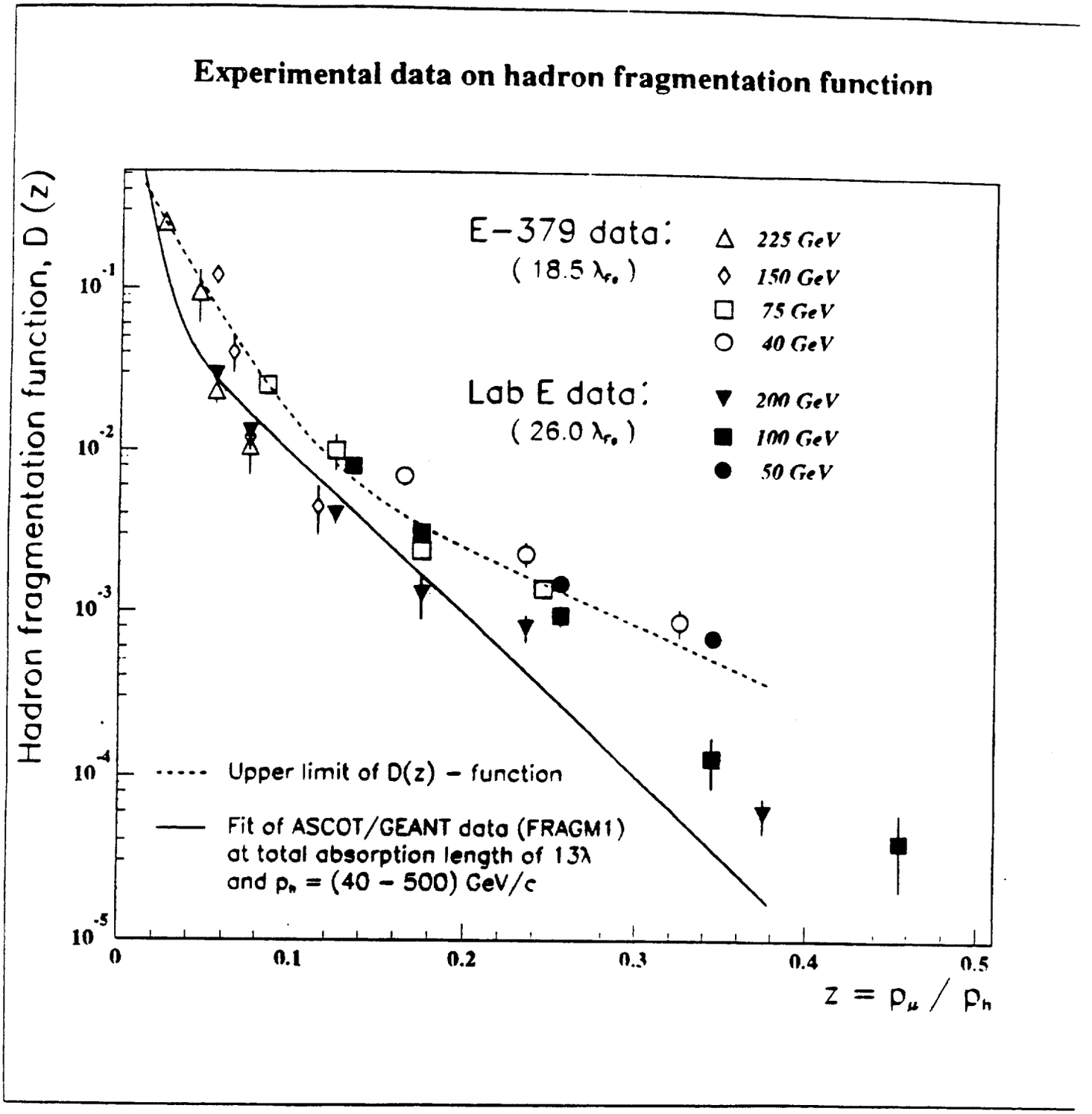

Figure 6: Data from Lab E experiment on $h \rightarrow \mu$ fragmentation function for 50, 100 and 200 GeV incident hadron energy (the total absorber thickness was $26\lambda_{Iron}$) and from E-379 experiment for 40, 75, 150 and 225 GeV ($18.5\lambda_{Iron}$). Solid line corresponds to our fit of ASCOT/GEANT data at 12λ and $p_h = (40 \div 500) GeV/c$.

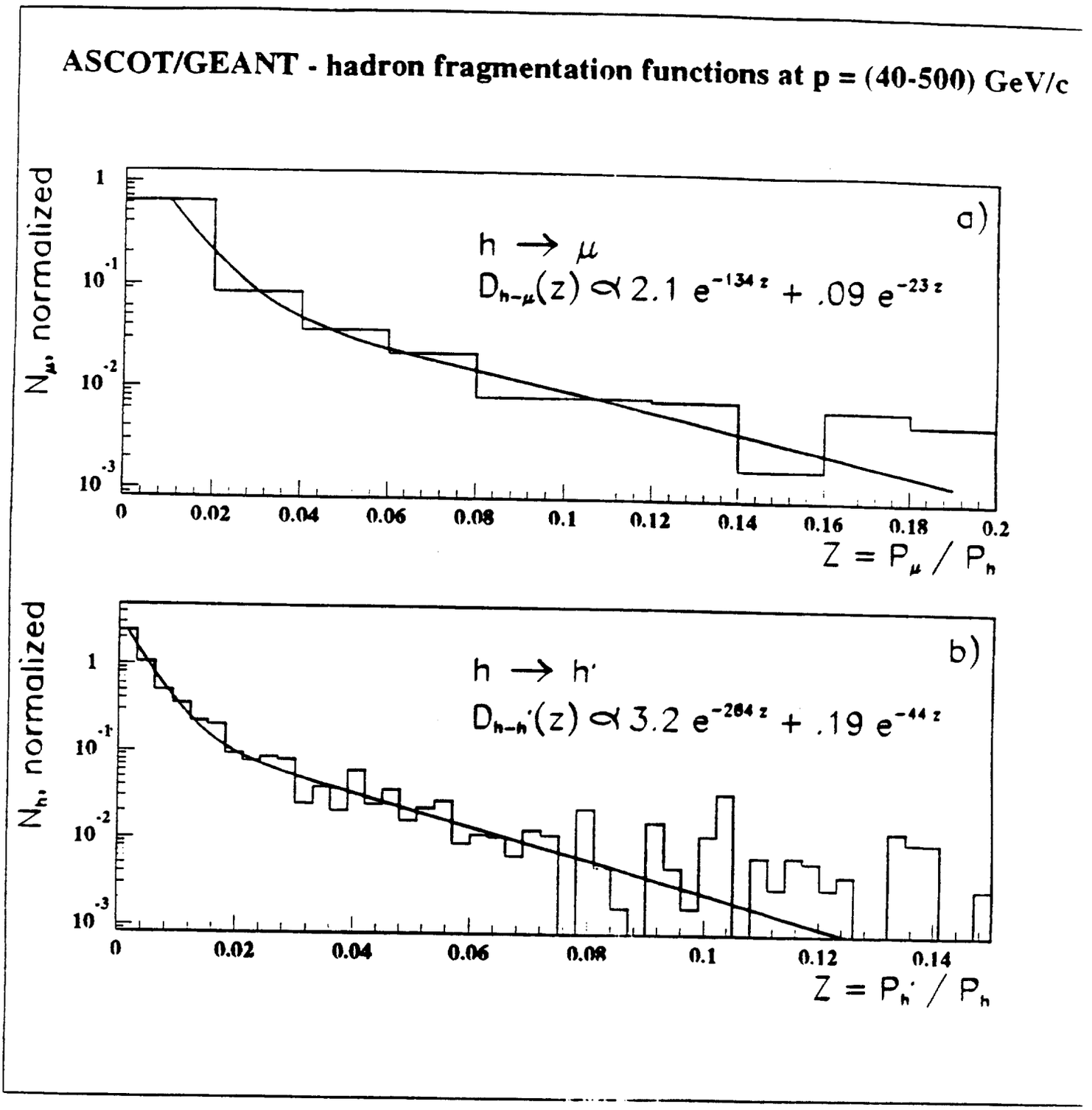

Figure 7: Fit of the hadron fragmentation function for muons (a) and hadrons from shower leakage (b).

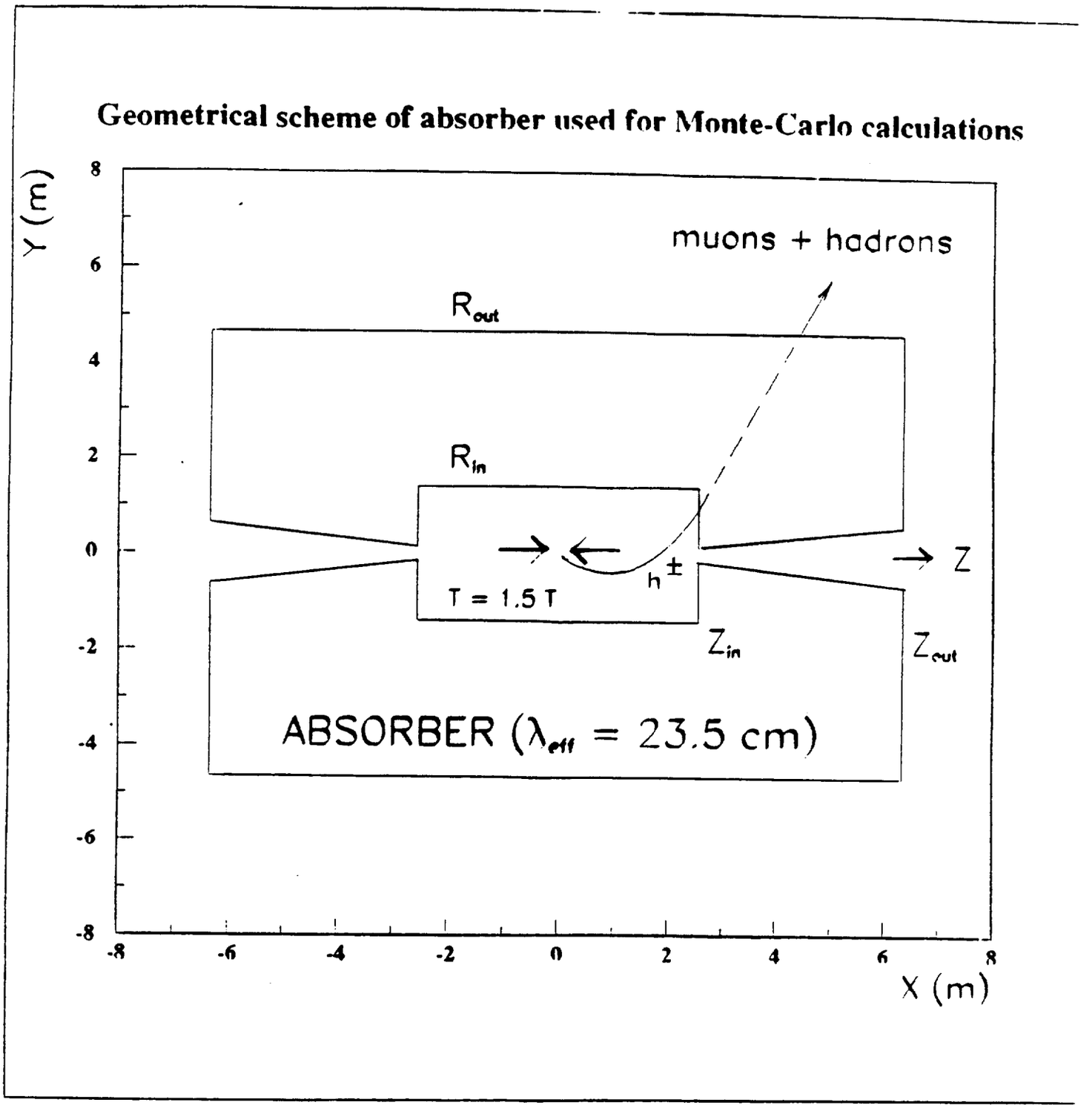

Figure 8: Scheme of geometrical calculation in the fast Monte - Carlo program.

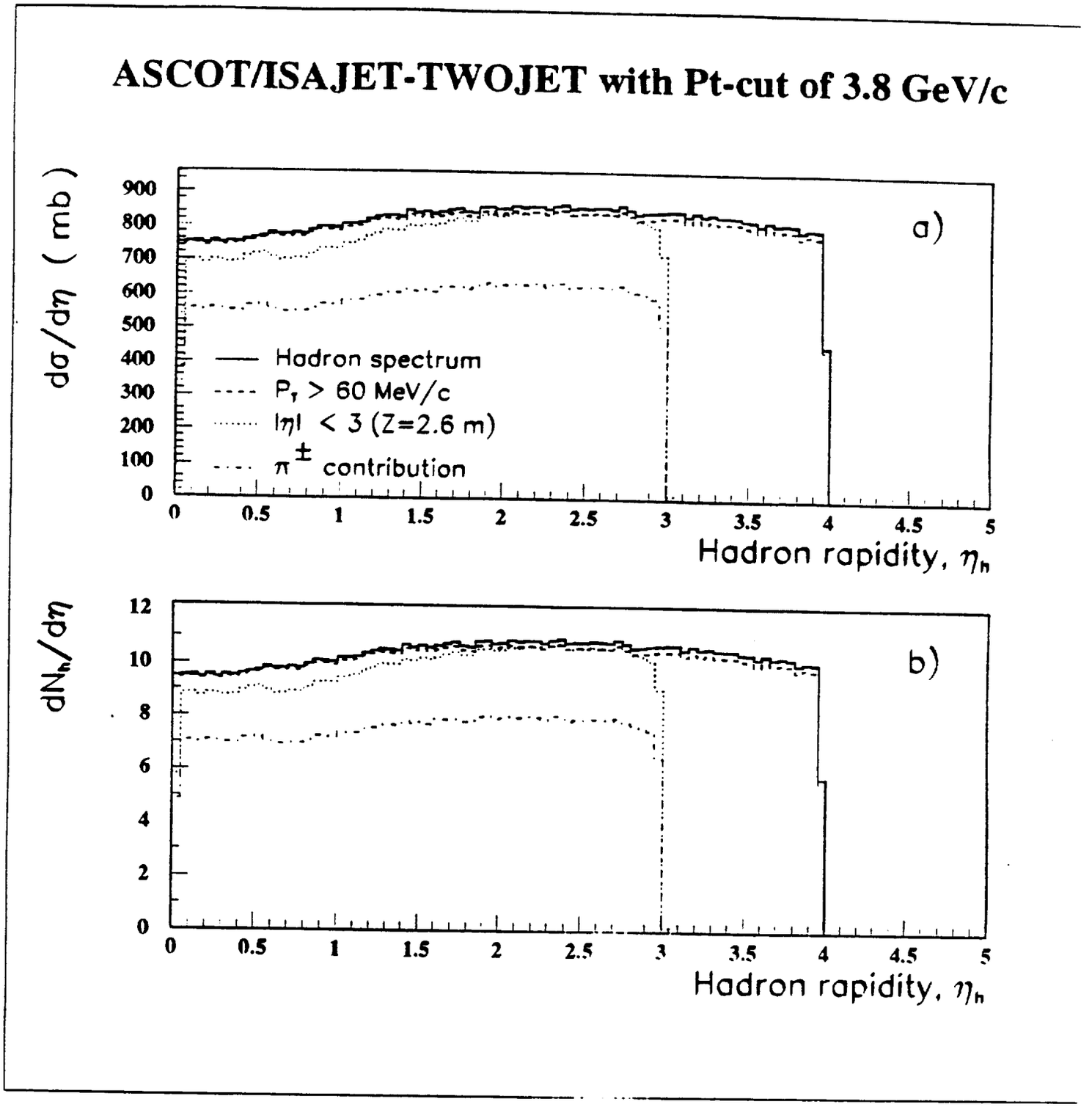

Figure 9: Rapidity spectra of hadrons which were produced in minimum bias events: a) differential cross section; b) number of hadrons per unit of rapidity. The influence of different "cut-off" criteria as well as charged pions contribution are presented.

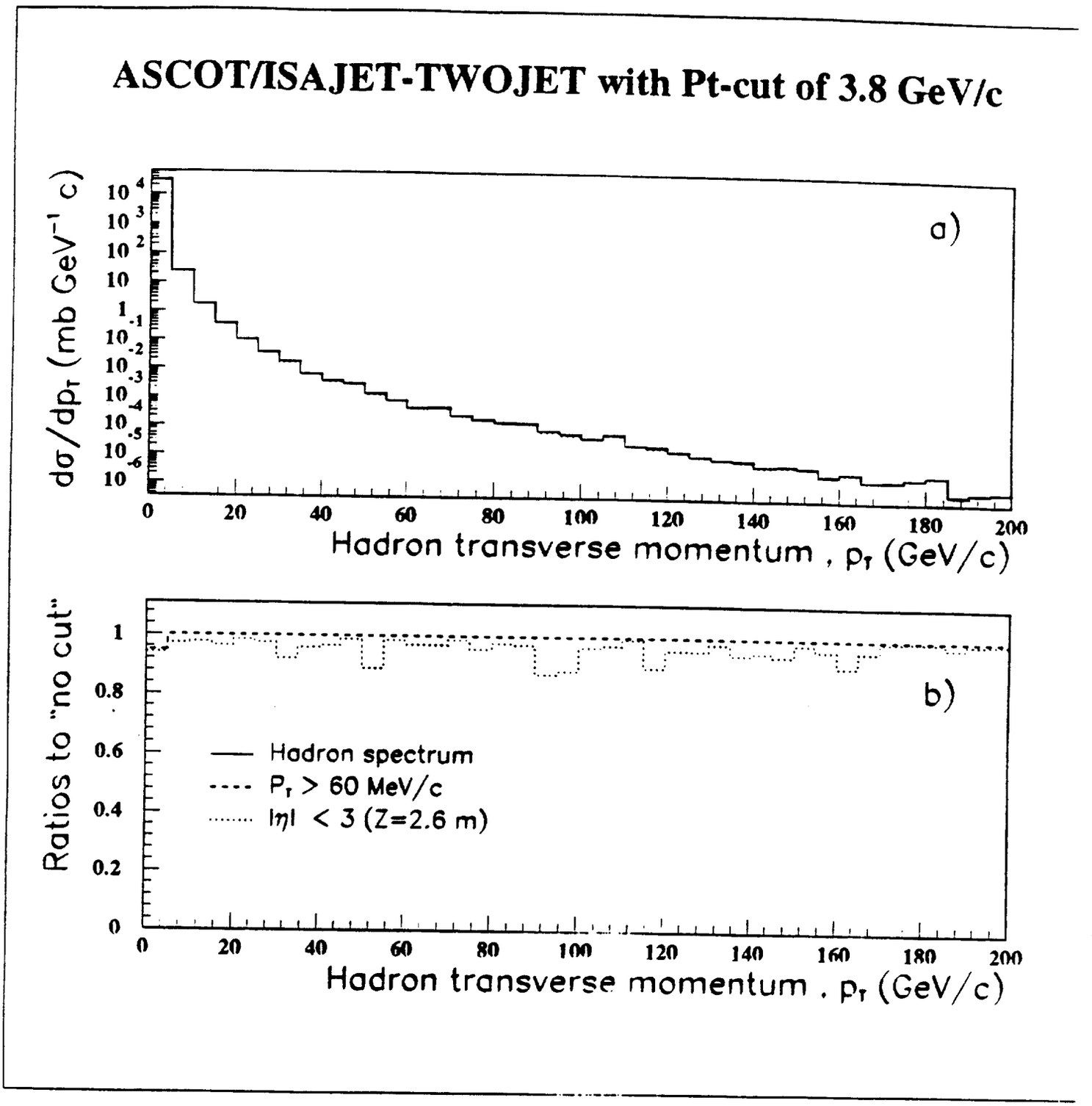

Figure 10: Transverse momentum distribution of hadrons in minimum bias events.

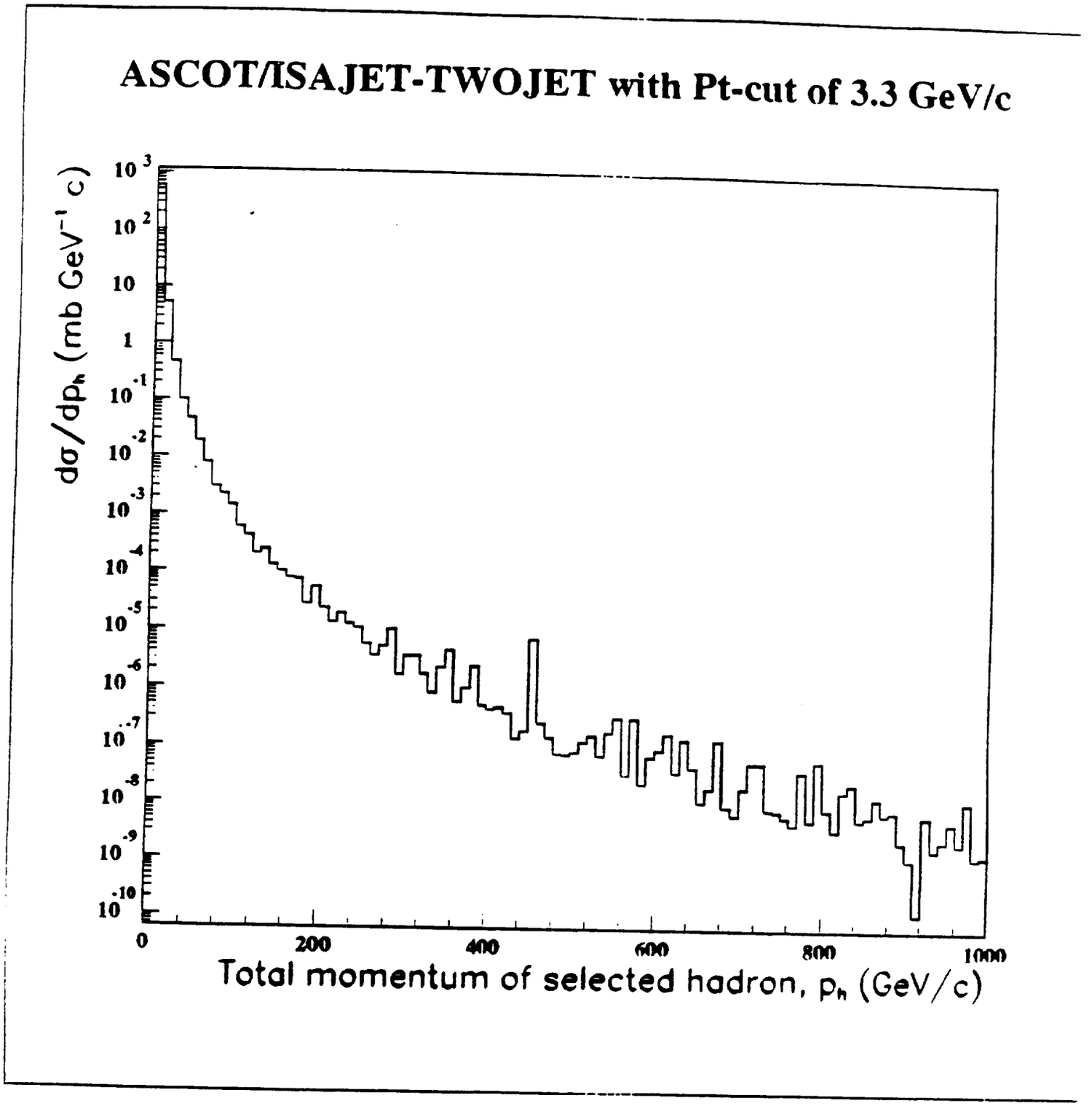

Figure 11: Momentum spectrum of selected hadrons which were used to generate muons and secondary hadrons.

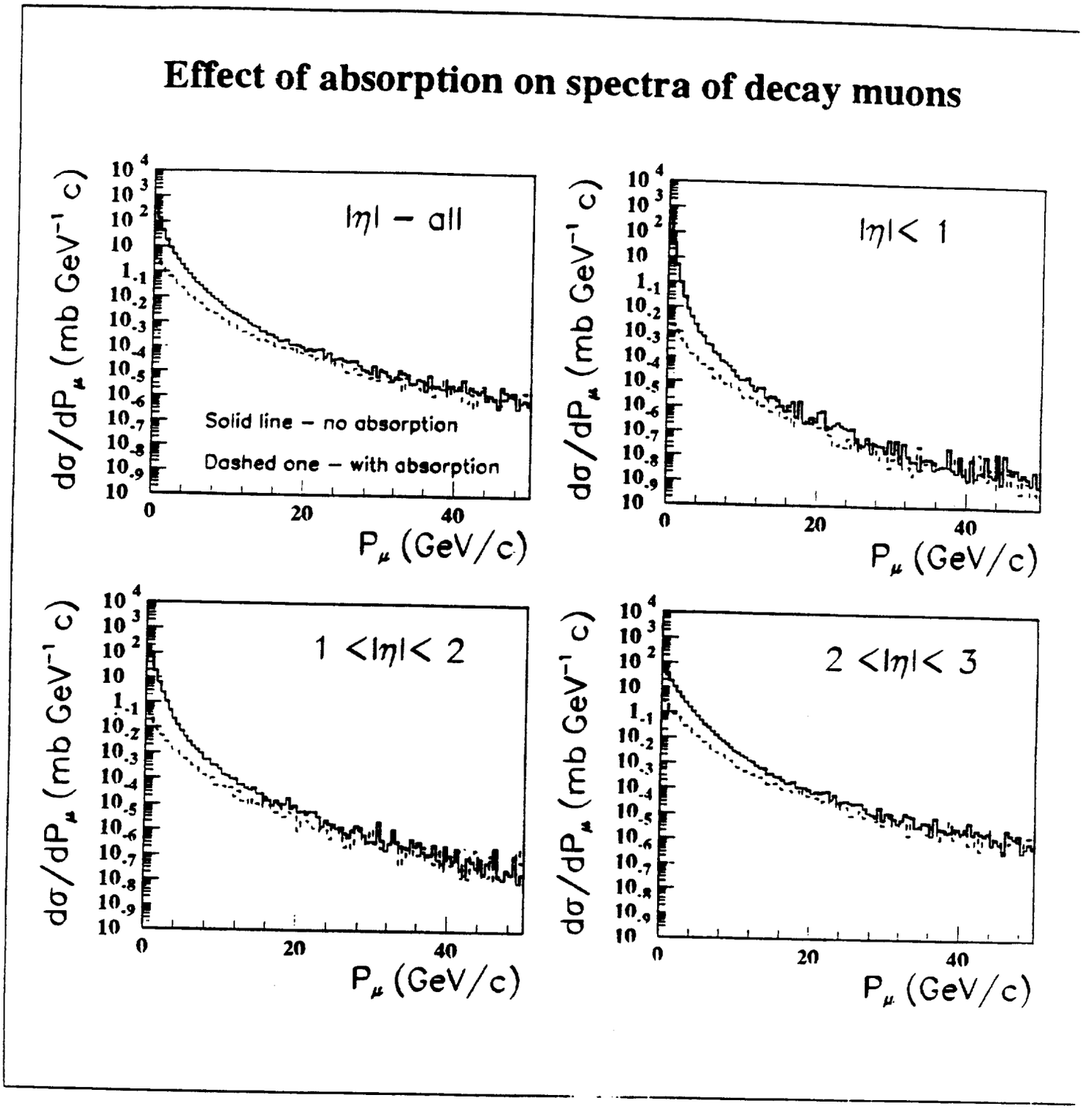

Figure 12: Comparison of muon momentum spectra from hadron decays with (dashed line) and without (solid line) absorption in the calorimeter.

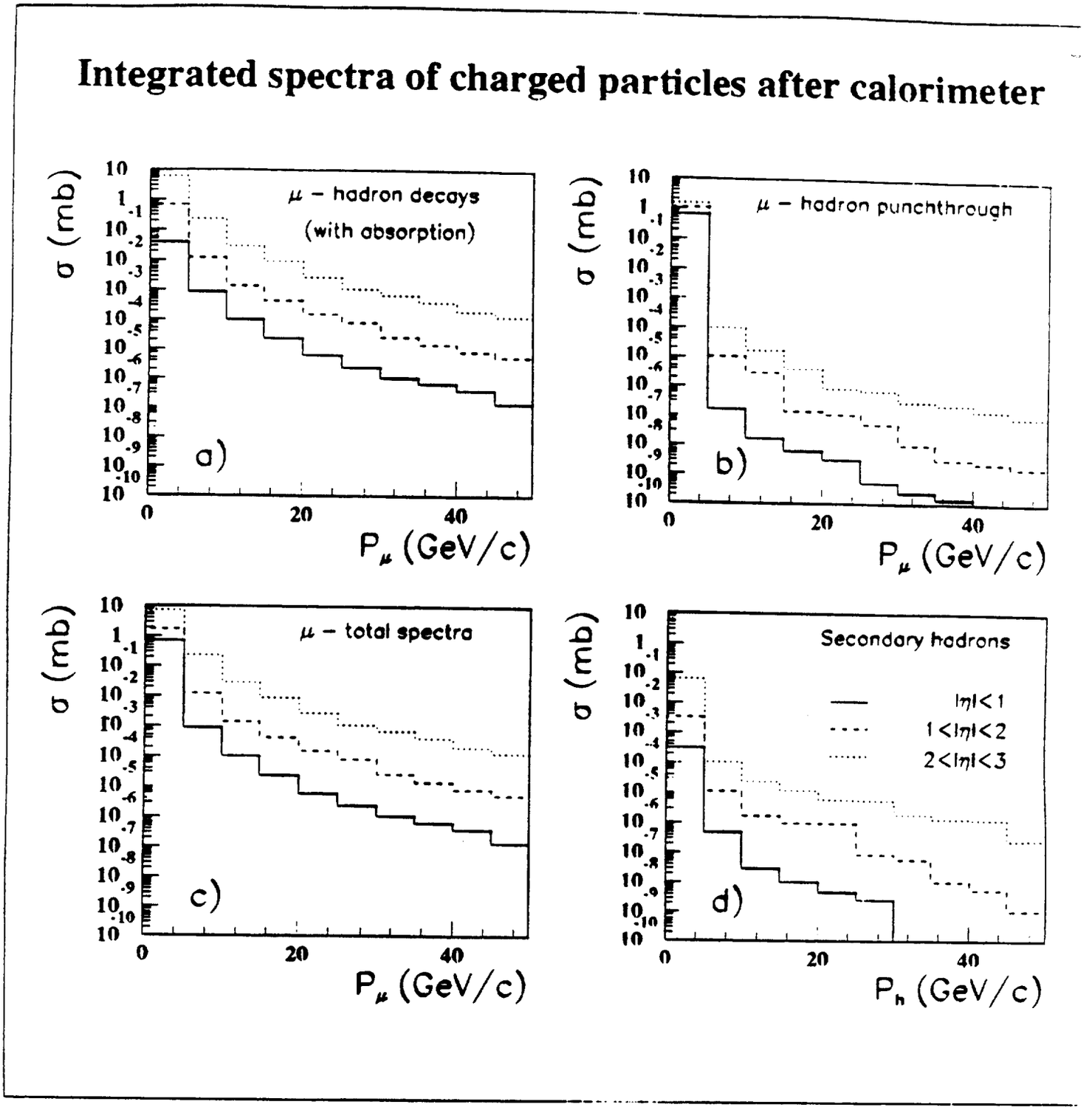

Figure 13: Integrated spectra of muons and hadrons produced in hadron decays and hadron punchthrough: (a) - for muons from hadron decays, (b) - for muons from hadron punchthrough (c) - summary muon spectra and (d) - for secondary hadrons.

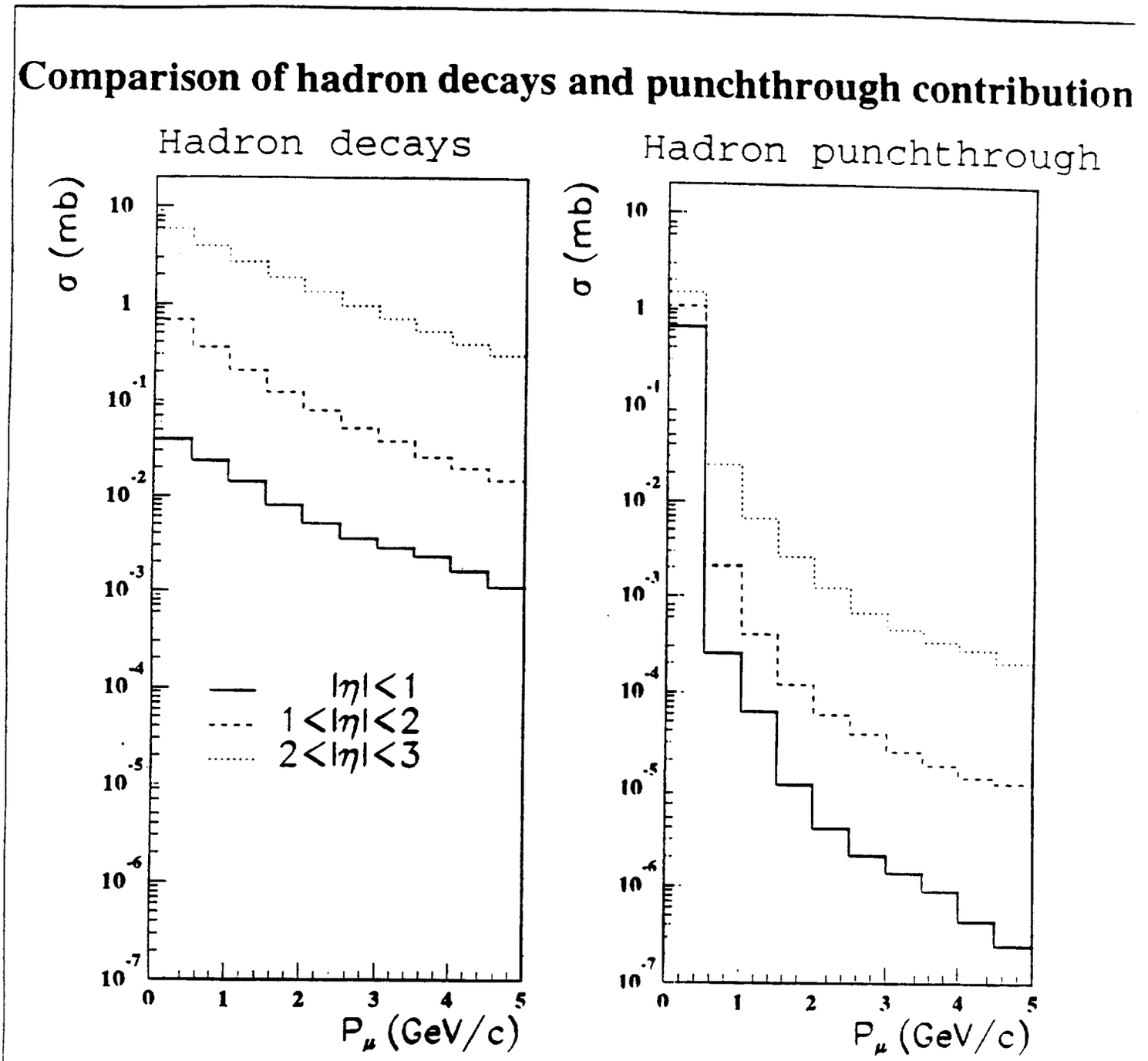

Figure 14: Comparison of muon spectra from hadron decays and from hadron punchthrough at the interval of small muon momenta.

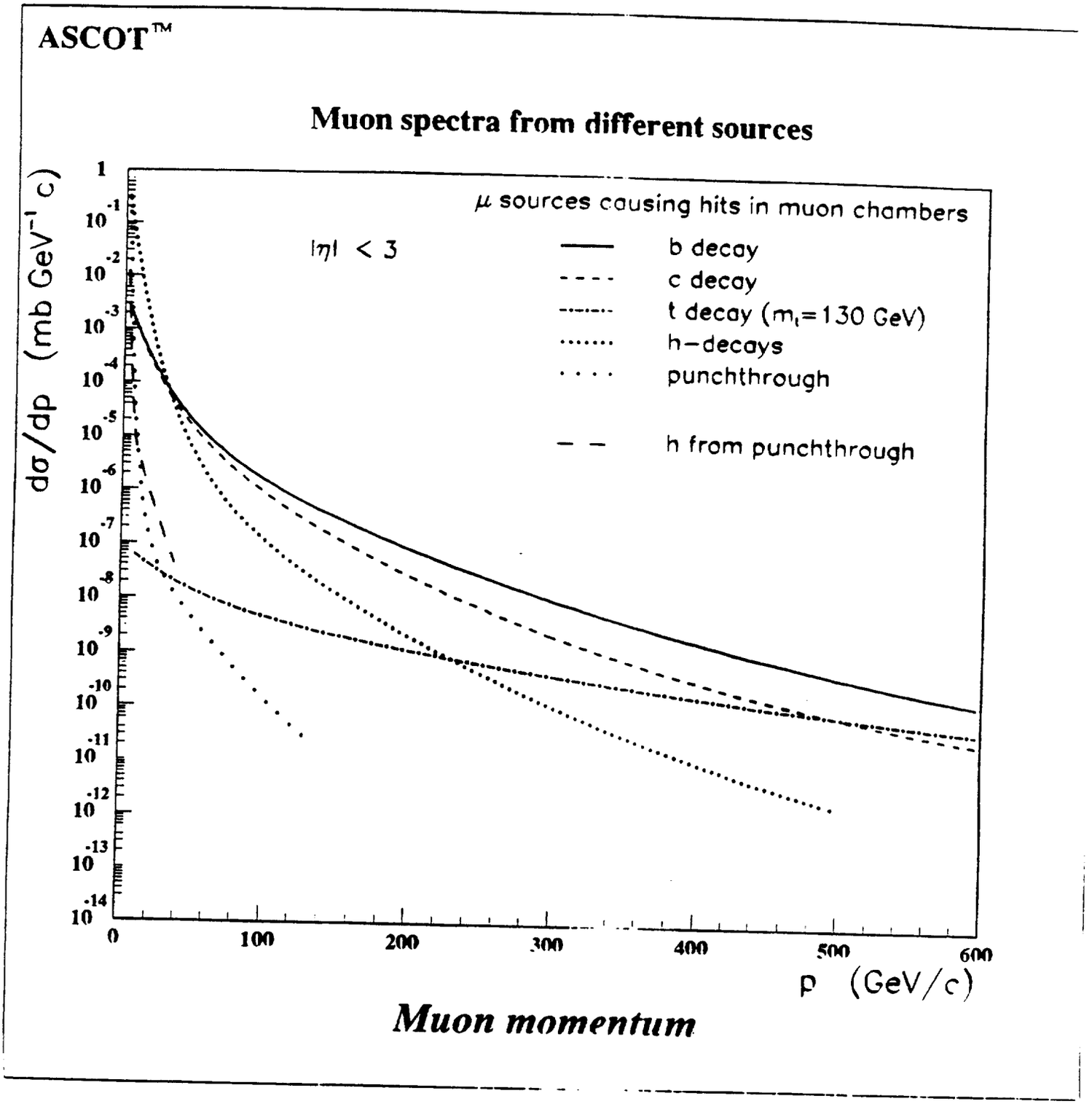

Figure 15: Comparison of differential muon spectrum from hadron decays and punchthrough with corresponding spectra from another sources.

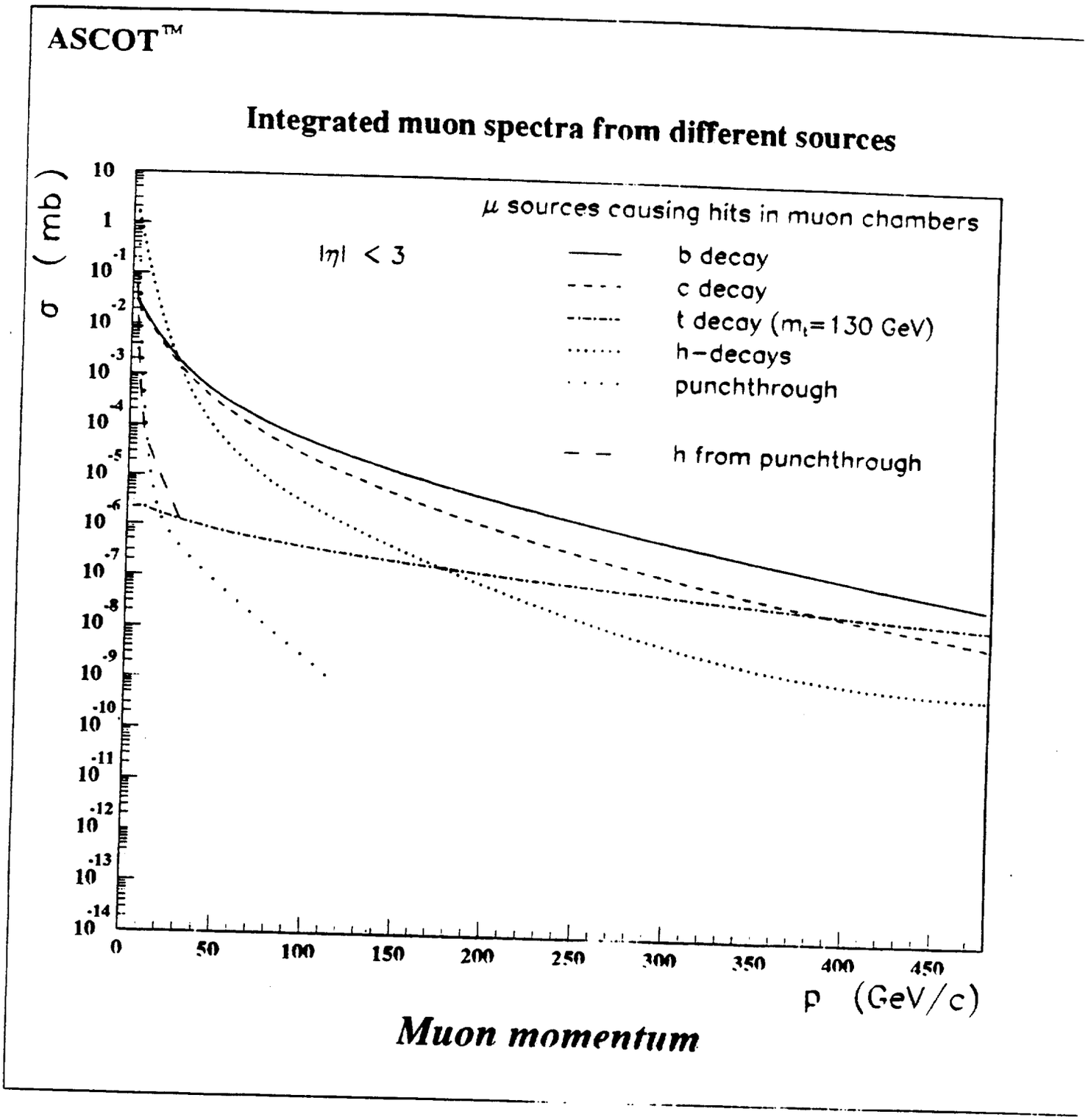

Figure 16: Comparison of the integrated muon spectra from different sources.

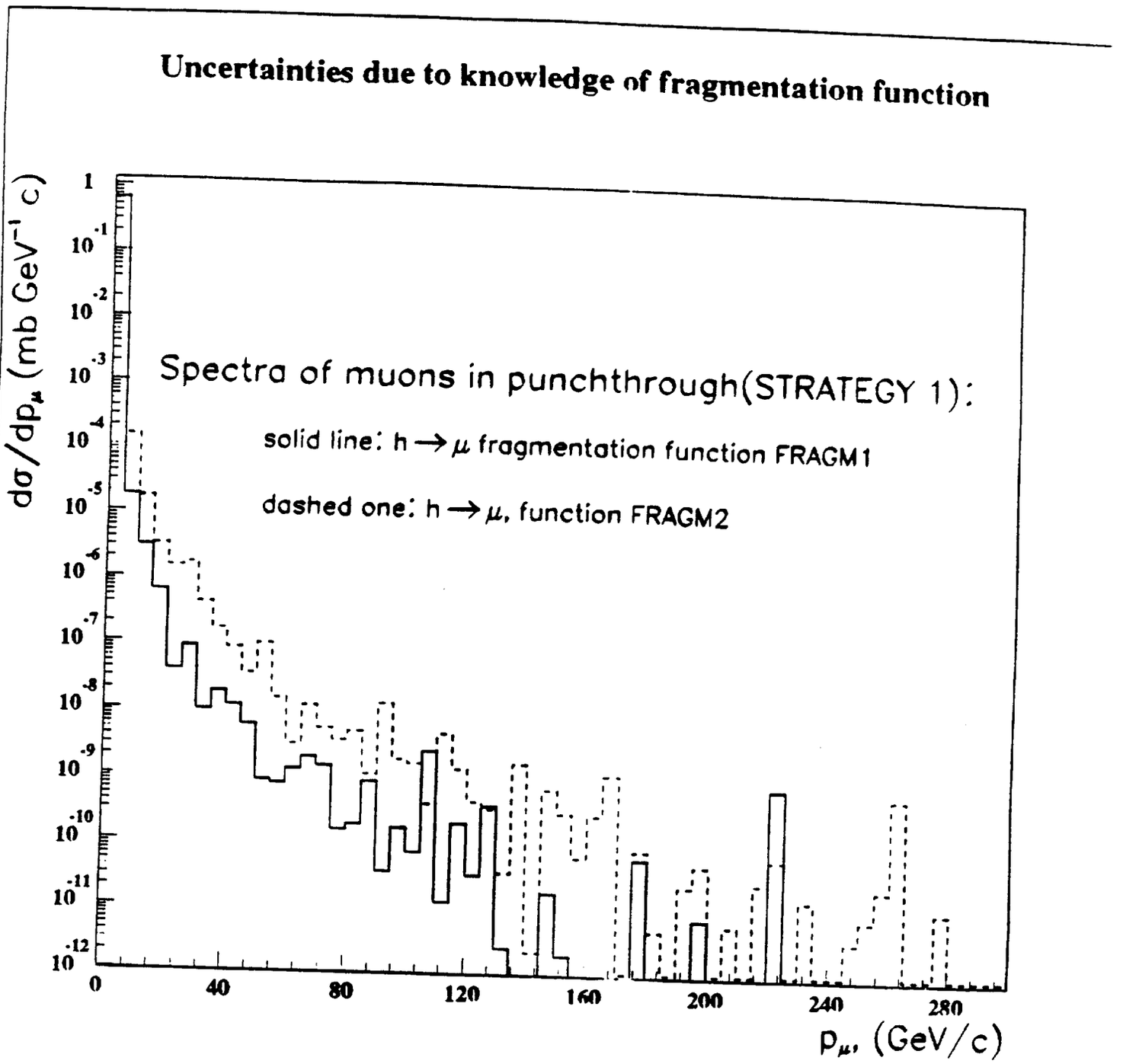

Figure 17: Comparison of muon spectra from hadron punchthrough for different fragmentation functions "FRAGM1" and "FRAGM2".

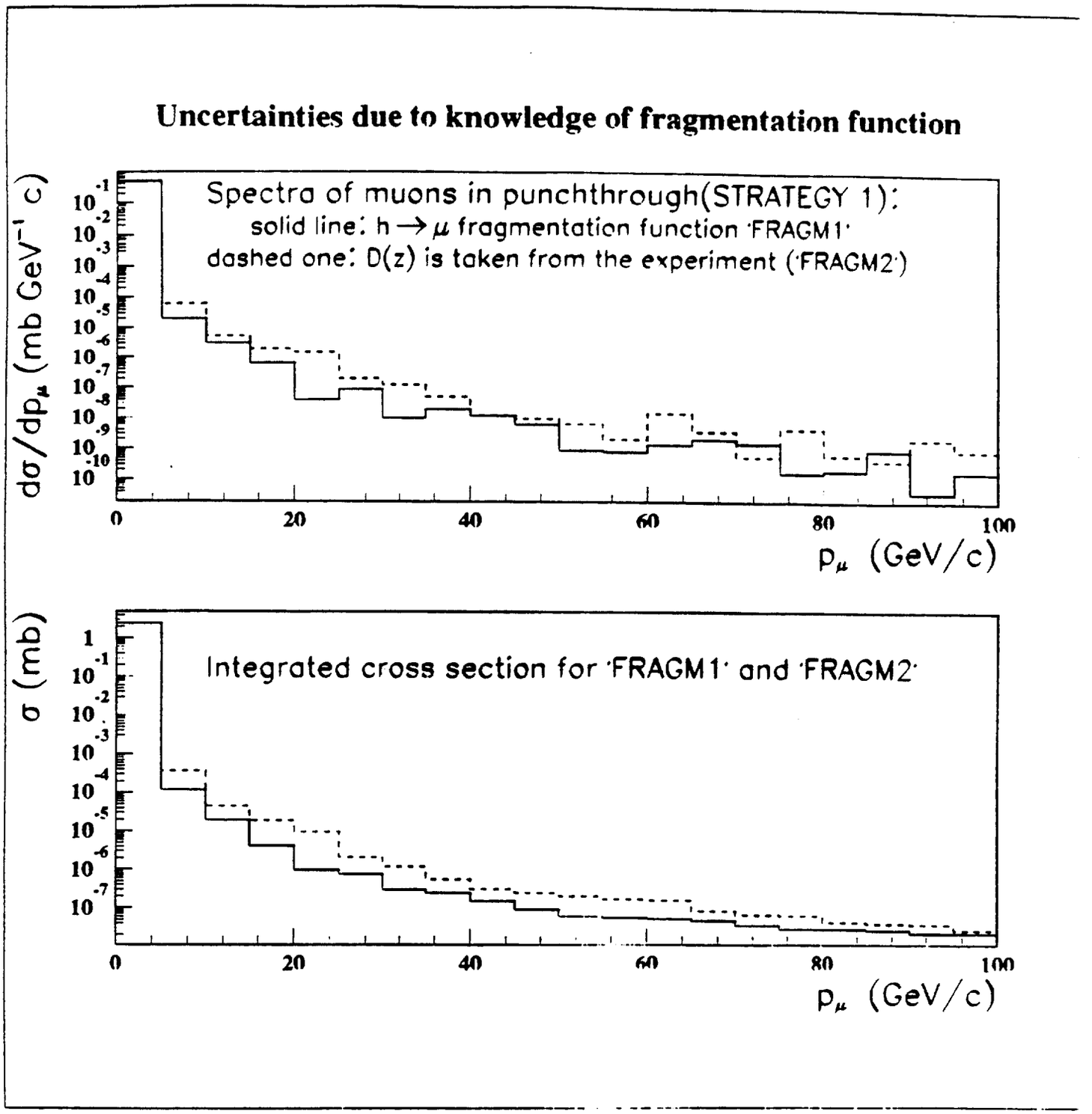

Figure 18: Comparison of muon spectra from hadron punchthrough for fragmentation functions "FRAGM1" and "D(z)". Function "D(z)" was obtained as upper limit of both lab E and E-379 experimental data.

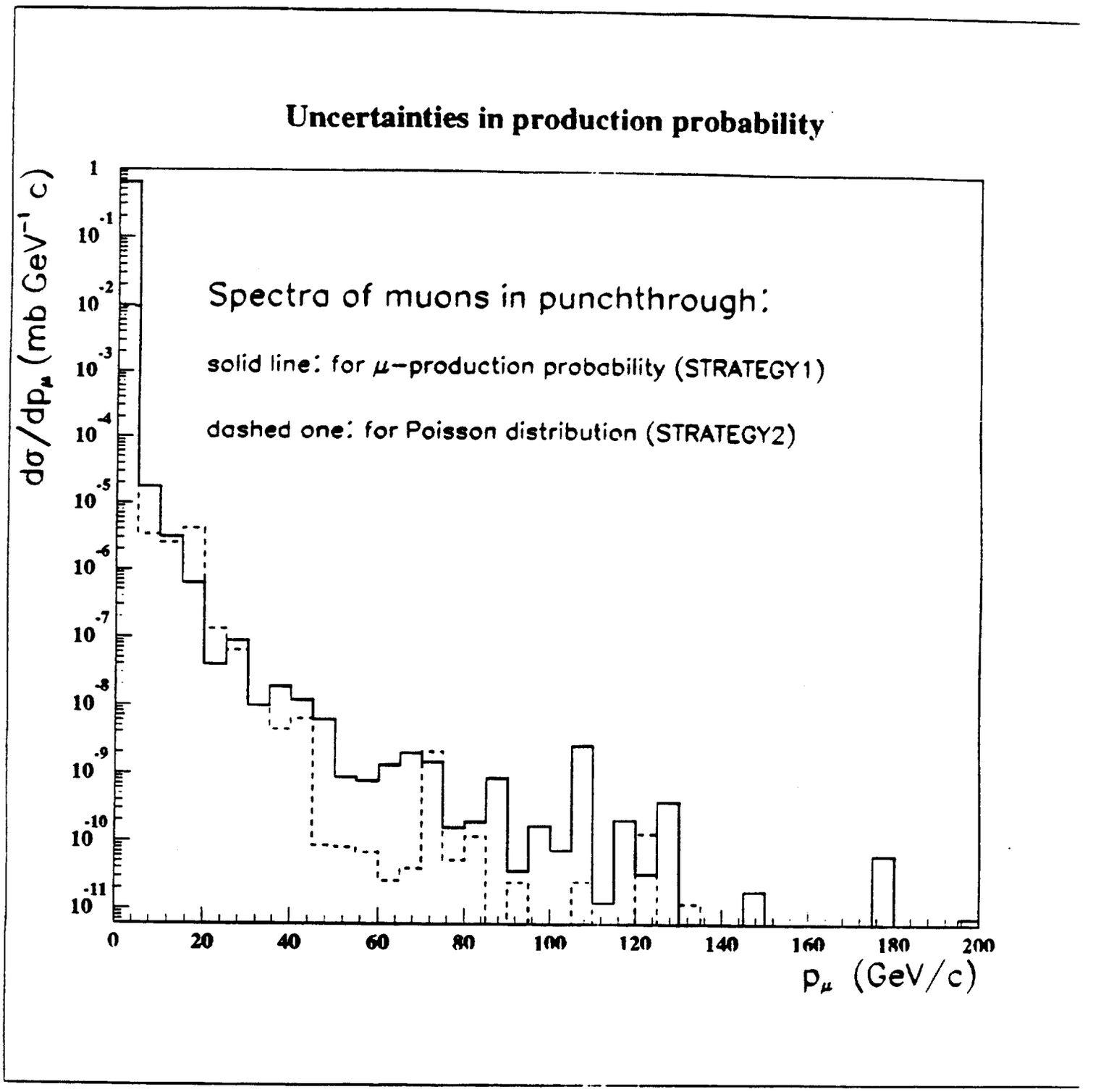

Figure 19: Comparison of muon spectra from hadron punchthrough for fragmentation function FRAGM1 and Poisson distribution usage.

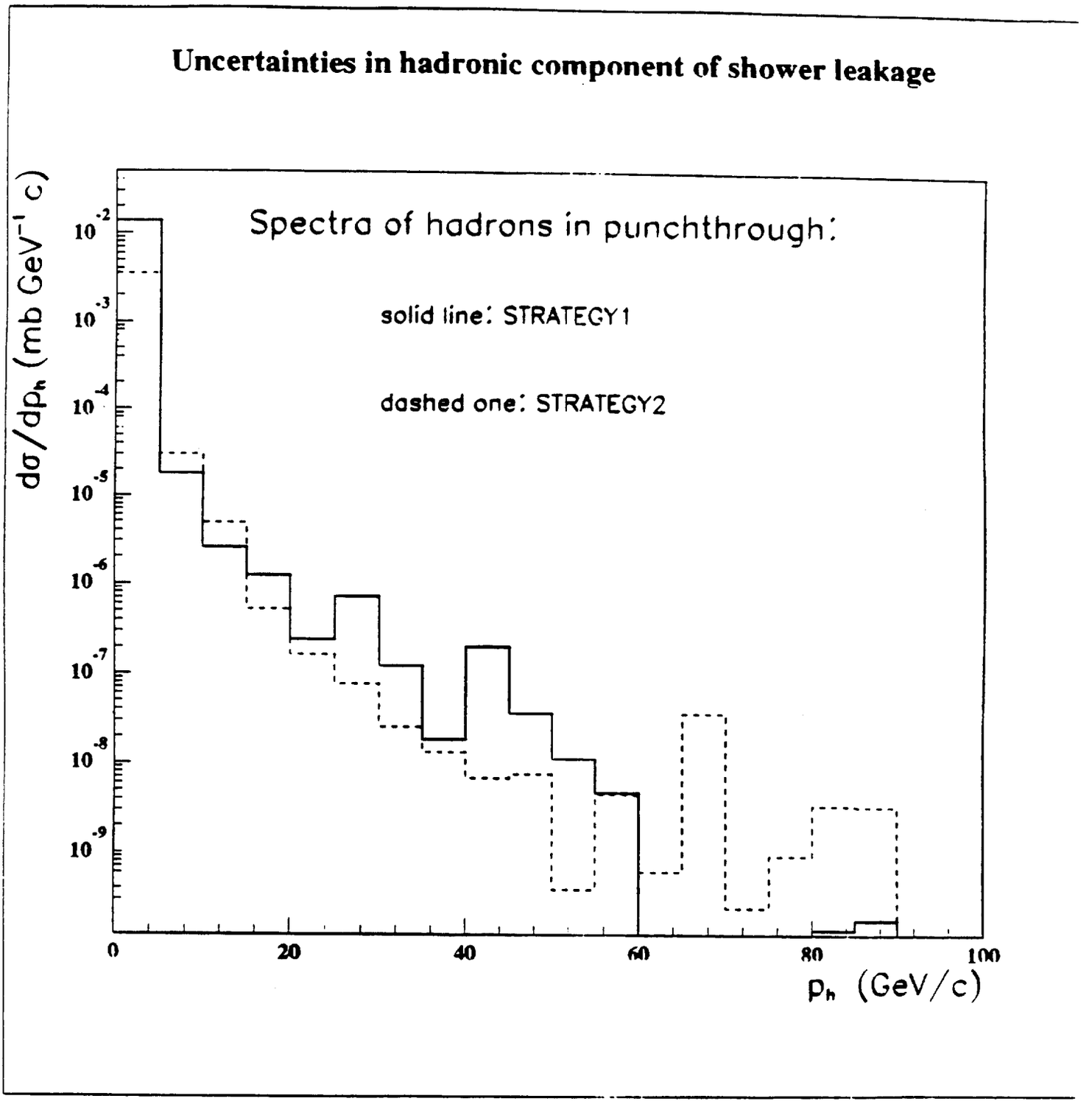

Figure 20: Comparison of hadron spectra from punchthrough obtained using fragmentation function as well as Poisson distribution.

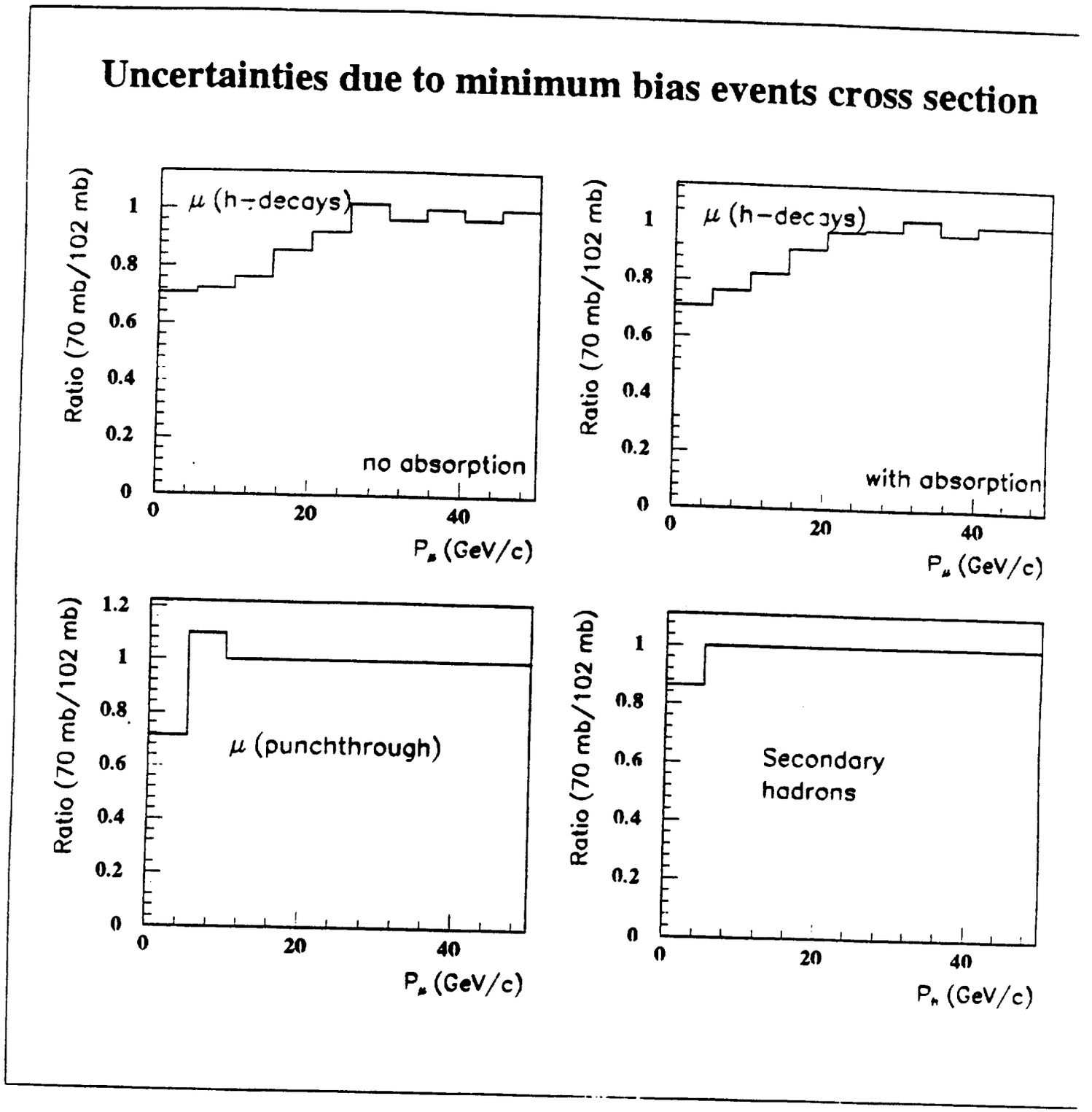

Figure 21: Ratios of muon and hadron momentum spectra obtained at lower limit to those at upper limit of the minimum bias cross section.

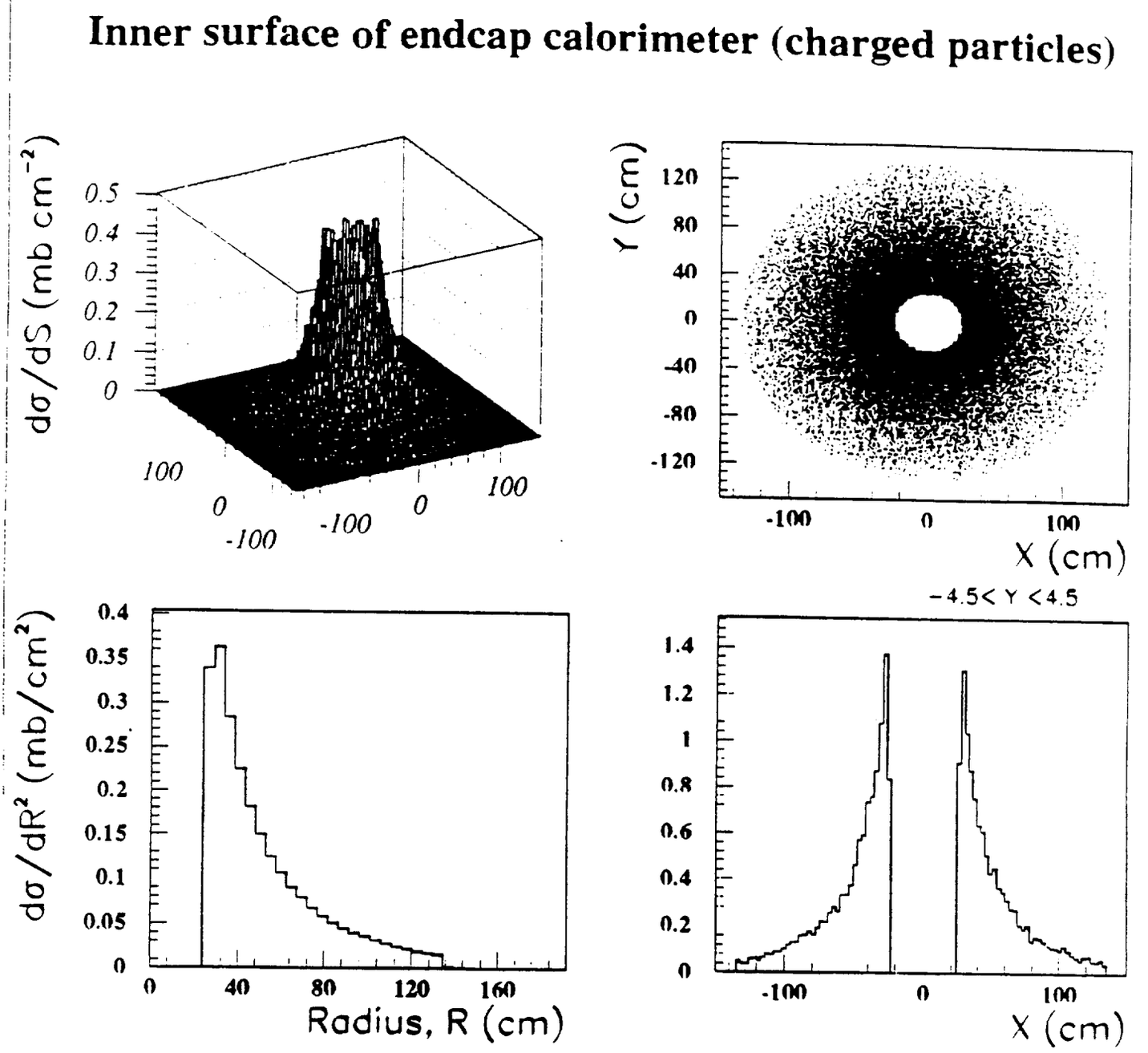

Figure 22: Different projections of the cross section of charged secondary particles on the inner surface of endcap calorimeter.

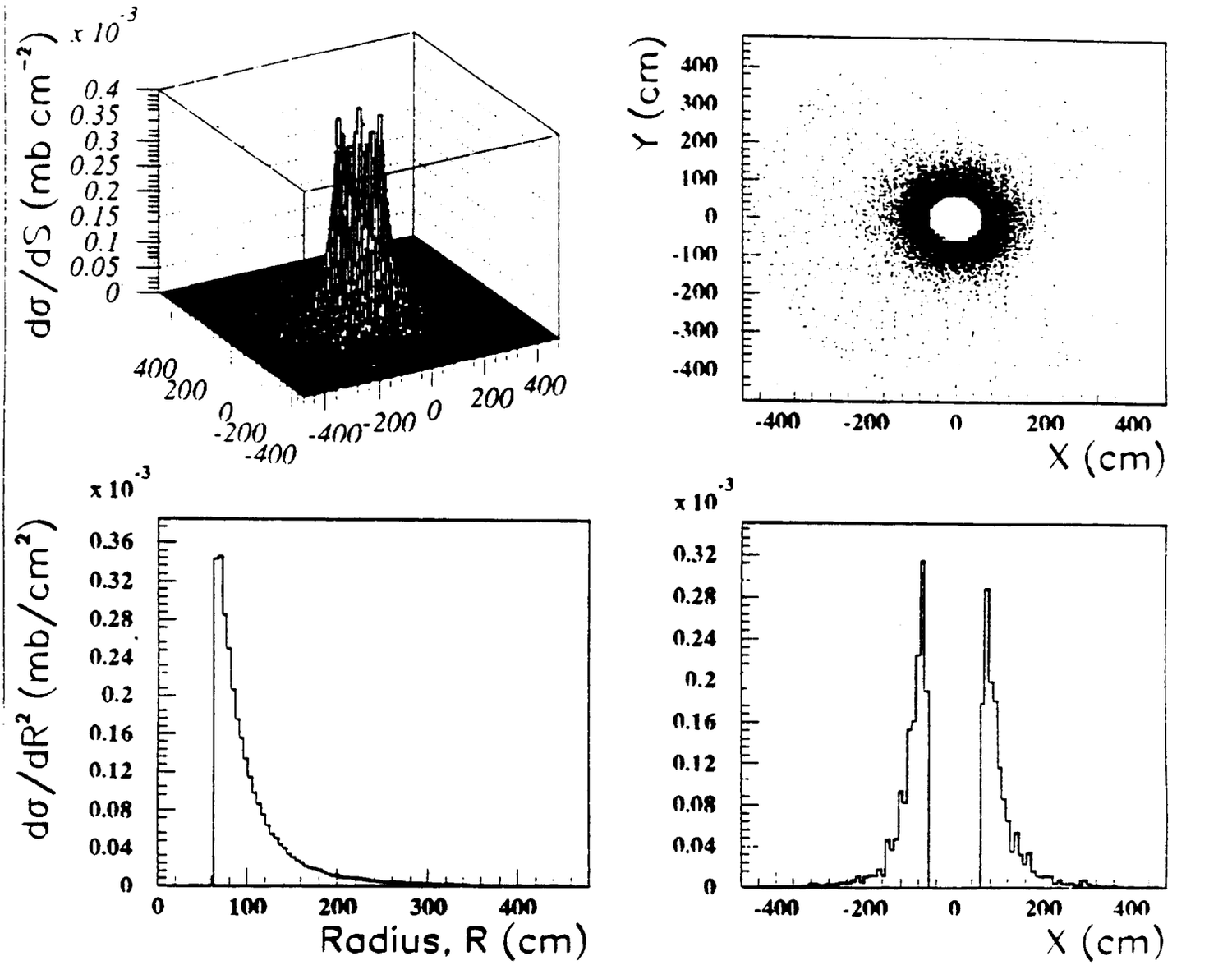

Figure 23: Different projections of the cross section of muons and secondary particles from shower leakage on the outer surface of endcap calorimeter.

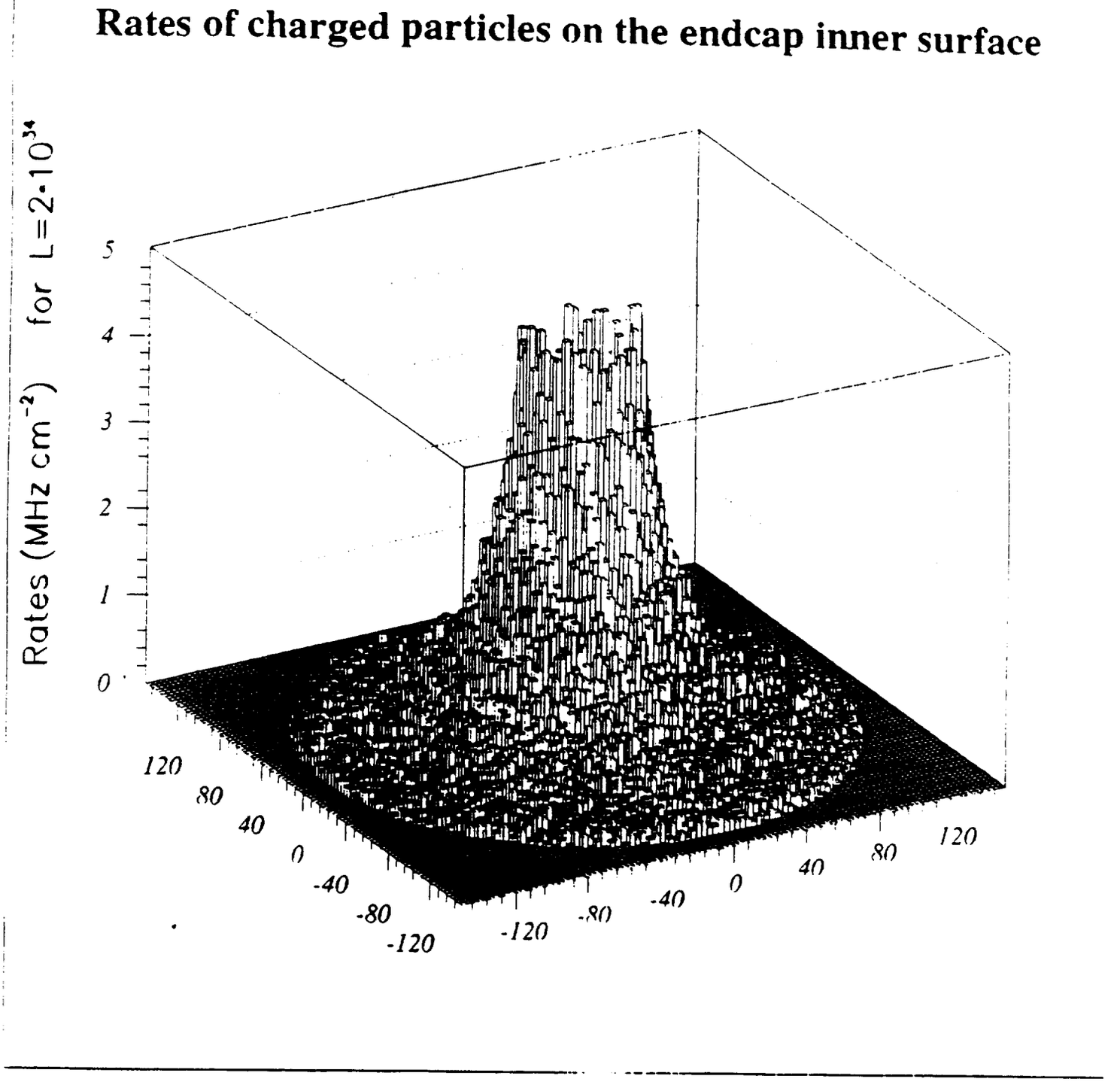

Figure 24: Rates charged secondary particles on the inner surface of endcap calorimeter.

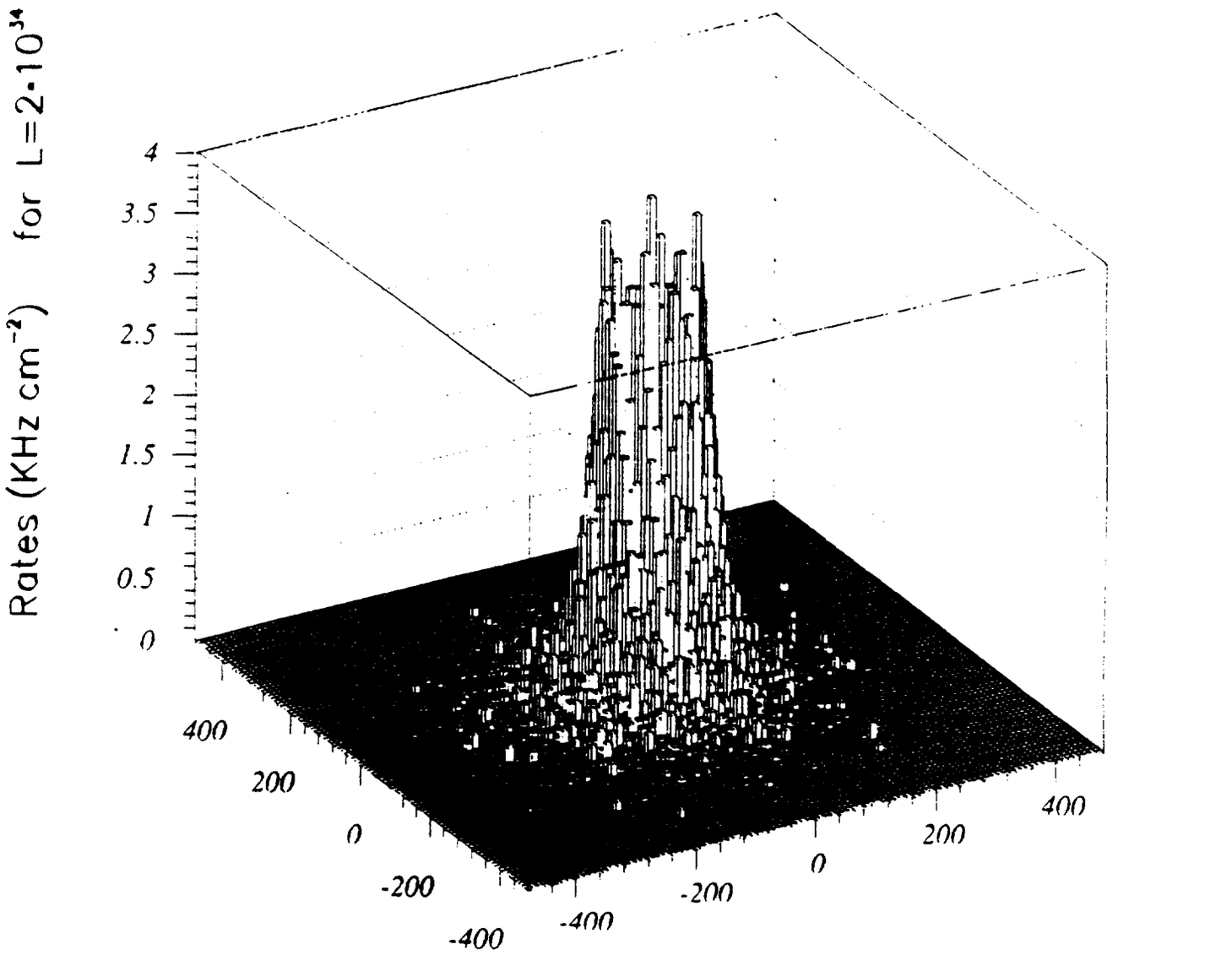

Figure 25: Rates of muons and charged particles from hadron shower leakage on the outer surface of endcap calorimeter.

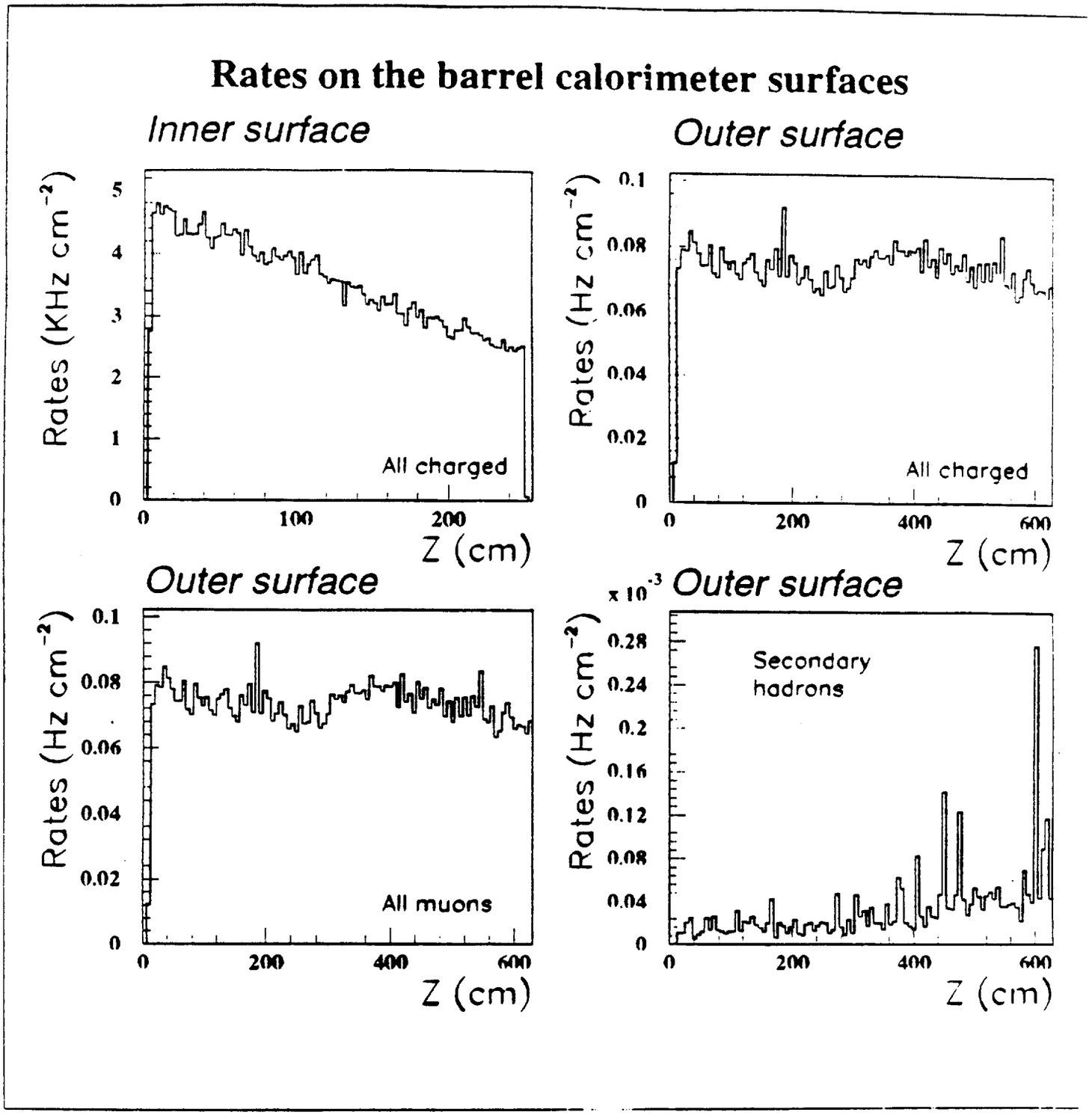

Figure 26: Muon rates on the barrel calorimeter surfaces.

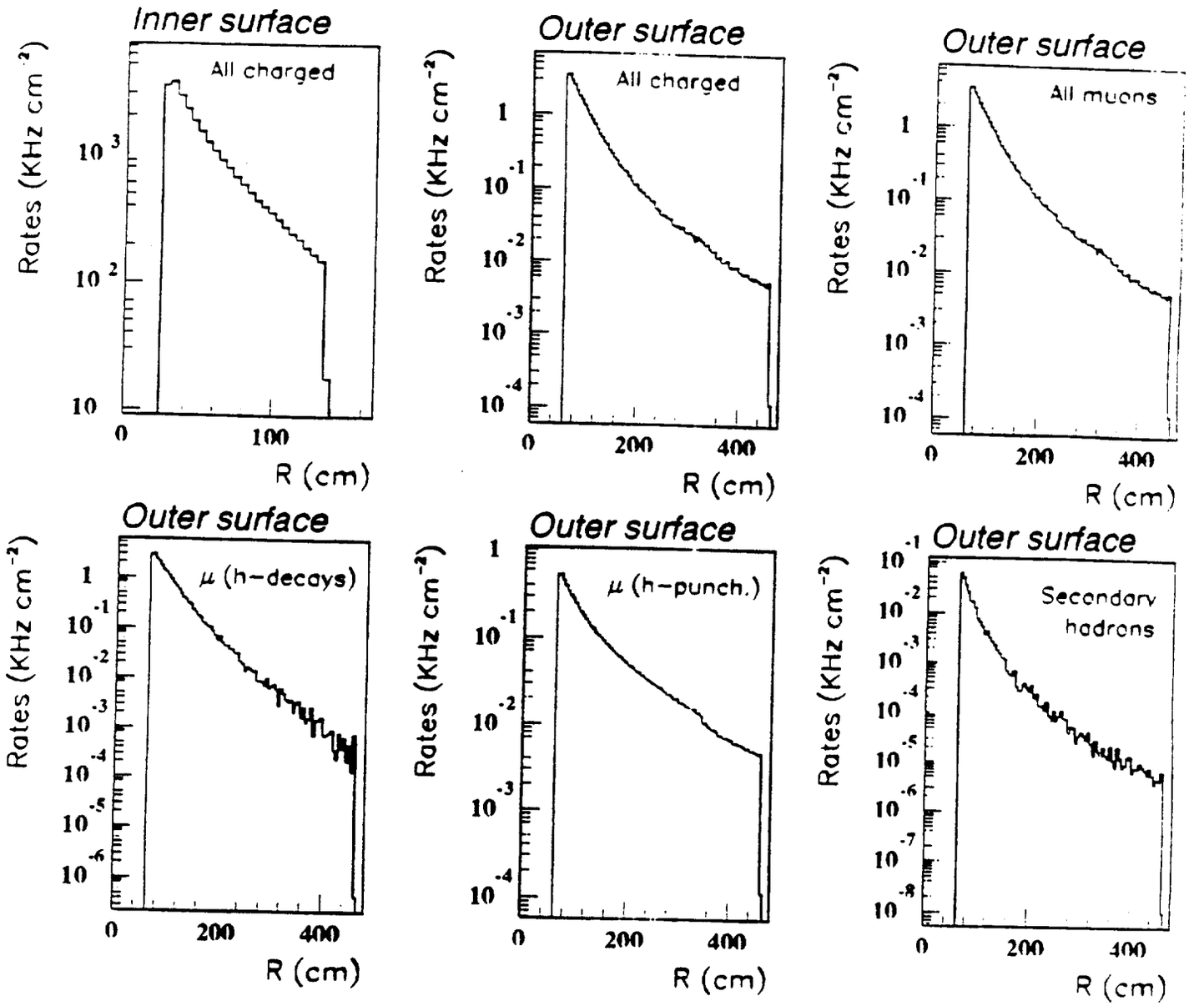

Figure 27: Muon rates on the endcaps.

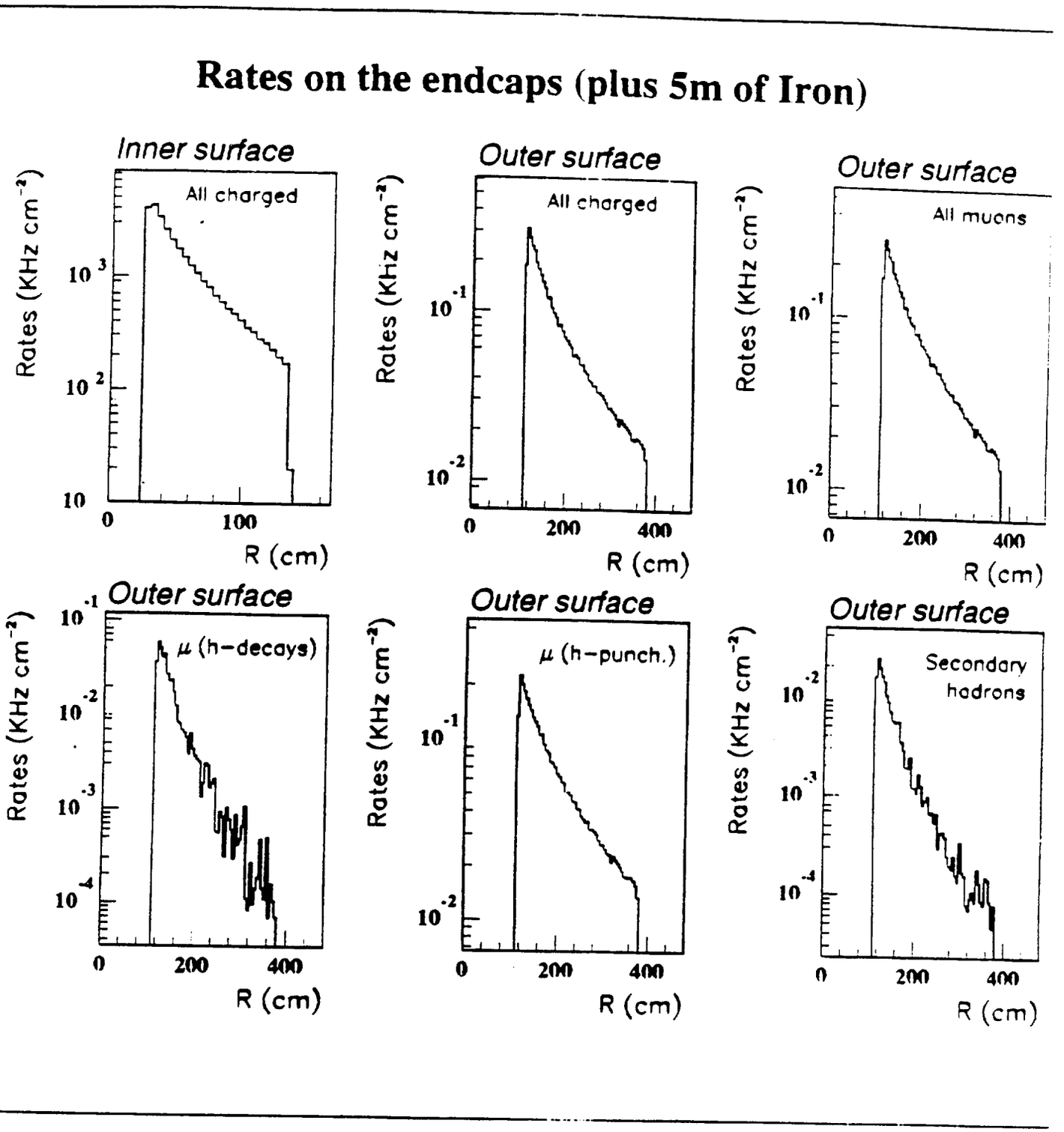

Figure 28: Muon rates on endcaps with additional 5m of iron absorber.

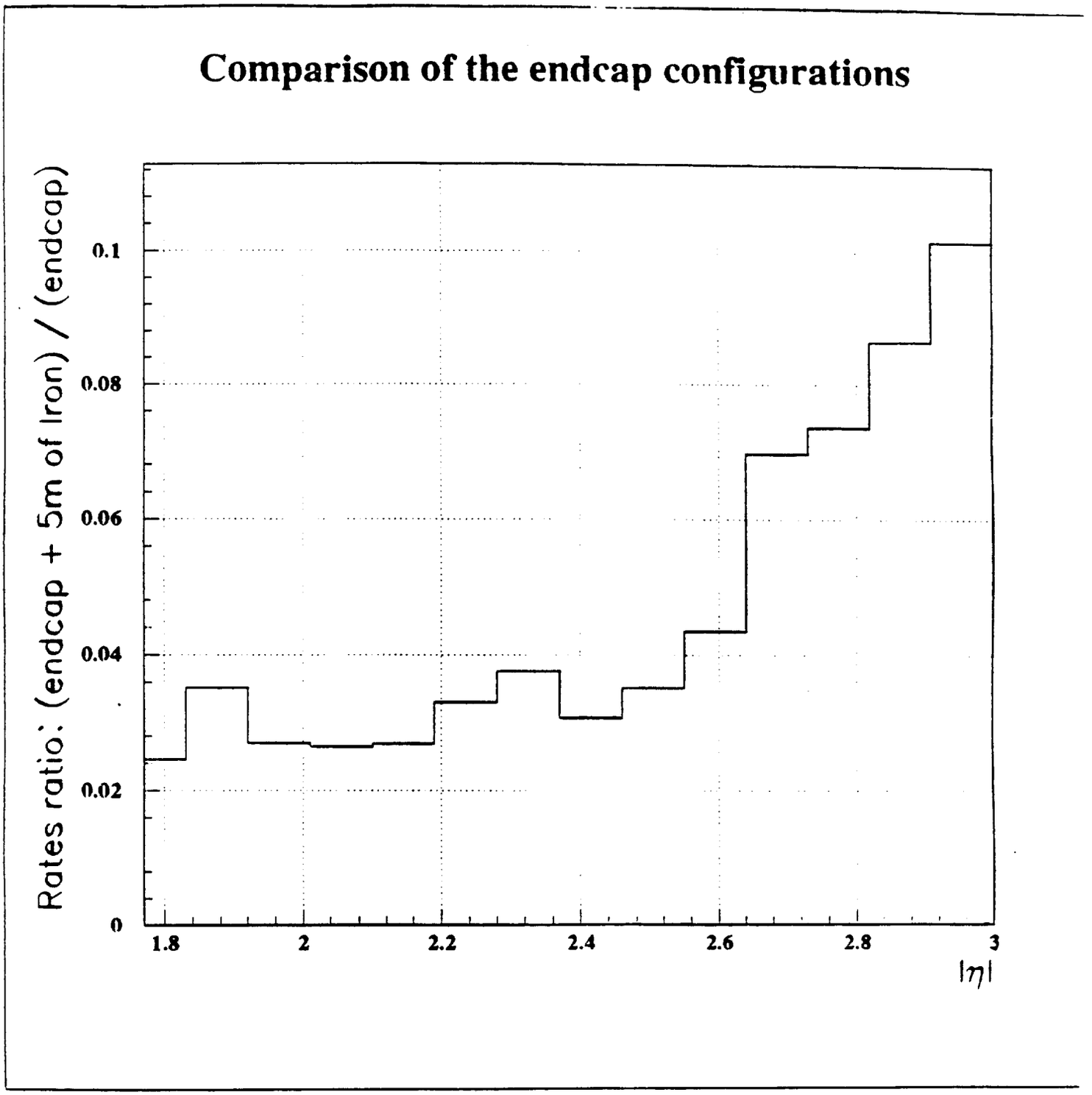

Figure 29: Rapidity dependence of the rates ratio with and without additional iron absorber.

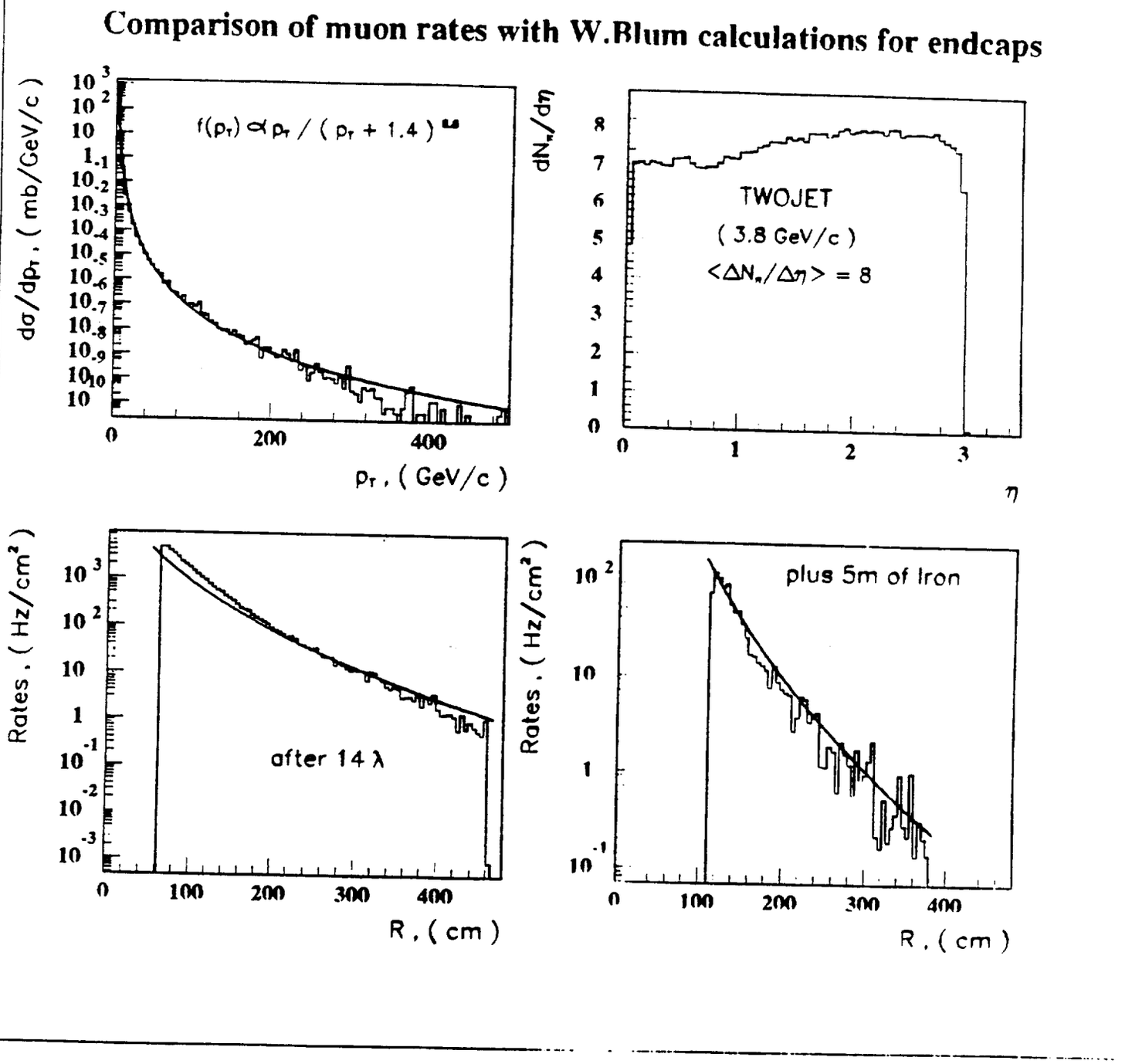

Figure 30: Comparison of muon rates from hadron decays with the calculations based on approximation of CDF experimental data.

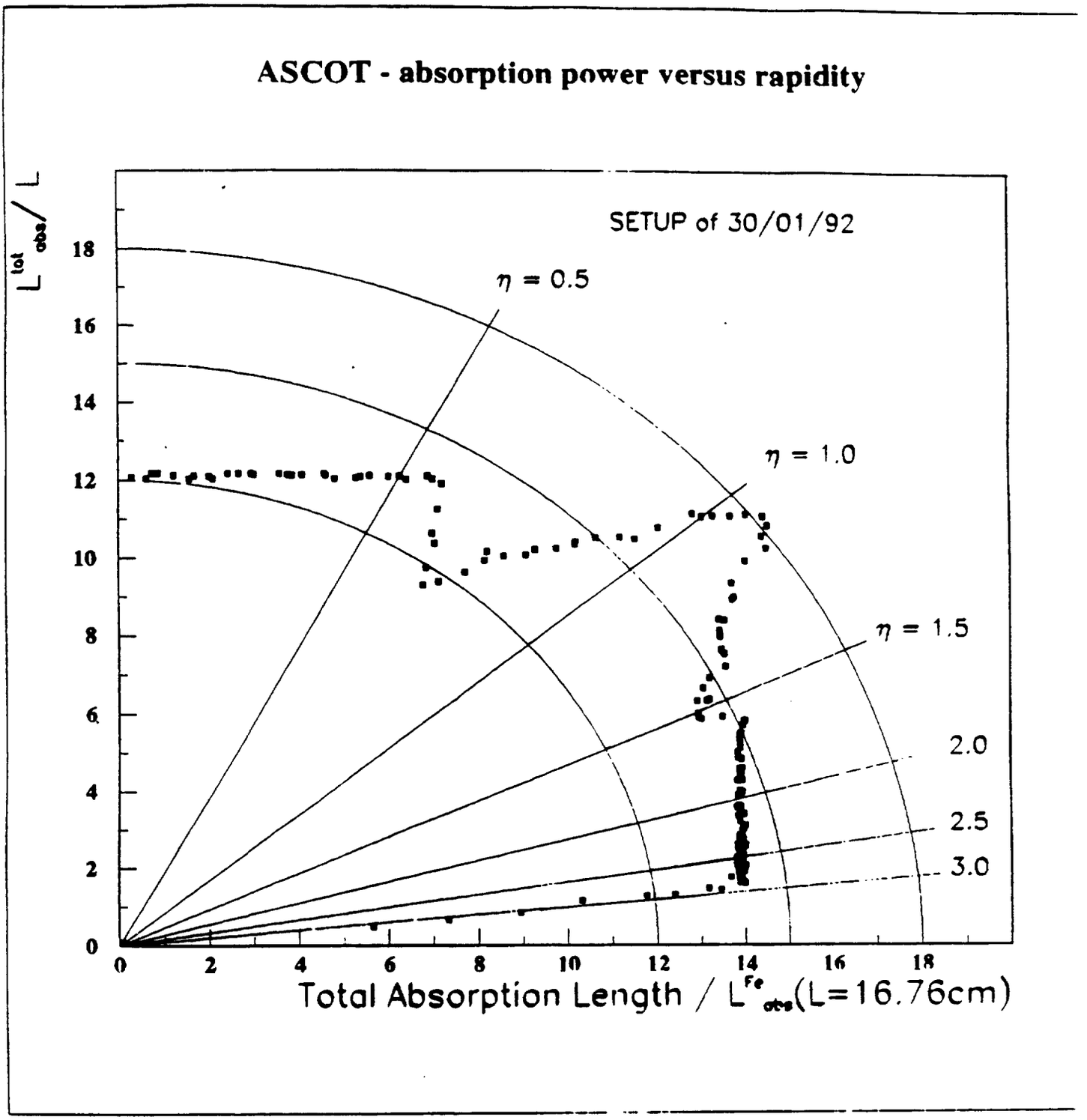

Figure 31: Total apsorption thickness of combined electromagnetic and hadron calorimeters and tail catcher for different rapidities (ASCOT Setup of 30/01/92).